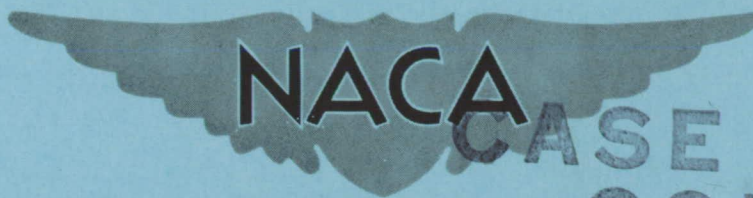


CONFIDENTIAL

Copy

372

RM E52112

CASE FILE  
COPY

## RESEARCH MEMORANDUM

INTERSTAGE SURVEYS AND ANALYSIS OF VISCOUS ACTION IN LATTER  
STAGES OF A MULTISTAGE AXIAL-FLOW COMPRESSOR

By William B. Briggs and Charles C. Giamati

Lewis Flight Propulsion Laboratory  
Cleveland, Ohio

CLASSIFICATION CHANGED TO UNCLASSIFIED

AUTHORITY: J.W.CROWLEY DATE: 9-15-55

CHANGE NO: 3096

WHL

CLASSIFIED DOCUMENT

This material contains information affecting the National Defense of the United States within the meaning of the espionage laws, Title 18, U.S.C., Secs. 793 and 794, the transmission or revelation of which in any manner to an unauthorized person is prohibited by law.

NATIONAL ADVISORY COMMITTEE  
FOR AERONAUTICS

WASHINGTON

March 5, 1953

CONFIDENTIAL

NACA RM E52112

DOCUMENT ON LOAN FROM THE FILES OF  
NATIONAL ADVISORY COMMITTEE FOR AERONAUTICS  
LANGLEY AERONAUTICAL LABORATORY  
LANGLEY FIELD, HAMPTON, VIRGINIA  
RETURN TO THE ABOVE ADDRESS  
REQUESTS FOR PUBLICATIONS SHOULD BE ADDRESSED TO  
NATIONAL ADVISORY COMMITTEE FOR AERONAUTICS  
1215 H STREET, N. W.  
WASHINGTON 25, D. C.

## NATIONAL ADVISORY COMMITTEE FOR AERONAUTICS

RESEARCH MEMORANDUMINTERSTAGE SURVEYS AND ANALYSIS OF VISCOUS ACTION IN LATTER  
STAGES OF A MULTISTAGE AXIAL-FLOW COMPRESSOR

By William B. Briggs and Charles C. Giamati

## SUMMARY

An eight-stage axial-flow compressor having a design-stage pressure ratio of 1.23 was investigated to determine the character of the boundary layers in the last four stages. The over-all performance was determined at speeds from 40 percent to 100 percent design, and detailed interstage surveys were made for four different weight flows at both 50 and 100 percent design speed. The surveys were made radially at one circumferential position behind the guide vanes and behind each blade row from the fifth rotor back. The survey data are presented as plots of the axial and tangential velocity profiles from which the boundary-layer parameters of displacement and momentum thickness were calculated. An analysis of the variation of these parameters was made to show how flows which are imposed upon the main through flow affect fluid particles whose momentum has been depleted by viscosity. A statement of current qualitative ideas and the status of quantitative theory regarding the imposed flows was made. Pronounced velocity peaks did not occur at midchannel. It was found that low-momentum fluid particles are carried into the main stream flow, where energy is interchanged to promote homogeneity, instead of accumulating on the annulus walls to effectively constrict the passage as in duct flow.

## INTRODUCTION

The effects that viscosity impose on the flow through the latter stages of a multistage axial-flow compressor are incompletely understood. Investigators have in some instances reported serious flow blockages in the latter stages. The detrimental effects of boundary-layer build-up along the annulus walls and blade surfaces are usually given as an explanation. A compressor designer must have a detailed knowledge of viscous action so that each specific portion of the flow area may be tailored most advantageously. Since the knowledge at the present time is limited, designers must use some gross effect which makes the gross area through the rear stages greater than that indicated as necessary by perfect fluid calculations. If the values of the two boundary-layer parameters, displacement and momentum thickness, could be known when the area variation is being calculated, any of the various gross-effect schemes could be used and they would give the same configuration.

Investigations have been made to determine typical values of these parameters. Previously reported studies have, however, been stringently limited in their range. Reference 1 presents results from a four-stage compressor having a constant-diameter hub and casing and running at Mach numbers less than 0.15. The constant annulus area contributed to large peaks in the hub-to-tip velocity profiles of the third and fourth stages. Reference 2 presents data from a three-stage compressor also having a constant-diameter hub and casing and operating at a low tip speed of approximately 120 feet per second. The annular wall boundary layers were reported as being relatively constant in thickness from a position ahead of the guide vanes to one behind the last stator.

The investigation presented herein was conducted at the NACA Lewis laboratory to extend this understanding of viscous effects. An existing eight-stage axial-flow compressor that had been designed for a tip speed of 925 feet per second and an over-all pressure ratio of 5.25 was used. Over-all performance runs were first made to ascertain the compressor performance. The compressor was then instrumented to permit interstage measurements throughout the last four stages and behind the inlet guide vanes. The guide-vane surveys were made to obtain a reference inlet value of the flow characteristics at each test condition. Unfortunately the casing could not be adapted to permit circumferential surveying behind the stators. All surveys made were on a radial line midway between two adjacent stator blades, and either slightly ahead of the leading edges or slightly behind the trailing edges. Behind the rotor this gives a circumferential average except for the presence of wakes which pass through the rotor from the upstream stator and which shift in circumferential position with changes in weight flow and speed. It is felt that stator wakes will have diffused sufficiently to cause only small deviations from the true circumferential average. Behind a stator, however, only conditions along the midline are obtained. These surveys behind the stators must be interpreted with caution and not as being the averaged values which a complete area survey would give.

The way in which the indicated boundary-layer parameters vary through the latter stages is shown and an analysis relates the various individual causes which contribute to the flow losses.

## APPARATUS

### Compressor Design

An existing eight-stage compressor having aluminum rotor, blades, and casing was utilized for this investigation. The hub and casing were those of the original NACA eight-stage axial-flow compressor that is described in reference 3. The compressor was made for a program unrelated to the one reported herein and sought to produce special velocity profiles entering an early, a middle, and a rear stage. To achieve this,

a bastard design was necessary because in some instances compromises of good over-all design practice had to be made. A design pressure ratio of 5.25 at 17.5 pounds per second and 925 feet per second tip speed was chosen. In calculating the stage variables, an adiabatic efficiency of 86 percent was assumed and no additional allowances for viscous effects, such as arbitrarily opening the annulus passage, were made. The blading was designed from cascade turning data reported in reference 4. Table I gives a tabulation of most of the pertinent physical characteristics. Figure 1 shows the details of the assembled compressor.

The physical arrangement of the air supply systems serving the compressor is schematically shown in figure 2. It is very similar to the setup recommended in reference 5 (figs. 1(a) and 2(a)) because the standard arrangements and methods of reference 5 were followed wherever they applied. The inlet duct, settling tank, and compressor were insulated. A calibrated adjustable orifice was used in the inlet duct to measure the mass flow. Motor-driven butterfly valves upstream of the stagnation tank and downstream of the collector controlled the inlet and outlet pressures at the compressor as well as the mass flow. Refrigerated air at a pressure of 10 pounds per square inch gage and any required temperature above 390° R as well as atmospheric air were available at the inlet to the system. A vacuum of 20 inches of mercury was maintained downstream of the outlet valve to exhaust greater quantities of air during the maximum mass-flow runs than would be possible with an atmospheric outlet. The compressor was driven through a speed-increasing gearbox by a variable-frequency electric motor.

### Instrumentation

Conventional instrumentation was installed for the determination of over-all performance. Four static-pressure taps, four total-pressure tubes, and four thermocouples were distributed in the stagnation chamber. Static-pressure taps were located in the compressor casing at four circumferential points behind each blade row. Total temperature was measured behind each stator row by fixed, 3/32-inch-diameter spike-type thermocouple rakes. Each rake consisted of three thermocouples spaced radially at one sixth, one half, and five sixths of the channel height. Total pressure and temperature in the constant-area annulus behind the last row were measured with two Kiel type total-pressure probes and two double-stagnation-type thermocouples fixed at different radial and circumferential positions. Also a static-pressure wedge and a ten-tube total-pressure rake, which covered the channel between two adjoining blades, were mounted in the outlet annulus in remotely controlled actuators; and radial variations were measured to give a mass-flow check on the orifice-measured flow and to give an integrated average outlet total pressure.

The motor speed was measured with a chronometric tachometer. The orifice pressures were measured on water manometers, the survey total pressures on tetrabromoethane manometers, and all others on mercury manometers. Temperatures were measured with a Brown potentiometer that had a dial calibrated to  $\pm 1/2^\circ$  F accuracy.

Semiautomatic instrumentation was developed for the interstage measurements to keep the running time required for each point from becoming prohibitive. Oblong mounting holes were made in the compressor casing to orient each mount parallel to the compressor axis and were so located that probes could be moved radially between the blade rows. It was impossible to adapt the casing for circumferential movement of the probes; therefore each hole was located equidistant from two adjacent stator blades and out of the path of wakes from the upstream stator row insofar as possible. For the principal body of data, a remotely controlled actuator was mounted after the guide vanes and one after each blade row from the fifth rotor back.

In figure 3 is shown an actuator holding an 1/8-inch-diameter claw total probe. The side tubes (claw) of the probe are connected to an automatically balancing capsule. A diaphragm in the capsule is deflected by the difference in pressure produced by misalignment of the probe with the flow so that an electric contact is closed, energizing the rotational motor which turns the probe into alignment. This maintains the tube in continuous alignment throughout a survey. Tees in the claw-tube leads went to a manometer in the control room affording a visual check. Prior to running, a program of survey points was built into an automatic radial positioner so that any or all probes could be quickly moved into position. This effected a large time saving with the slight handicap that some blade rows (after the sixth stator, for example) had to be surveyed with fewer points than might be desired. The angle and radial orientation of the probe were known at a remote place and were controllable through a potentiometer geared to the probe shaft and wired to similar potentiometers in the control room which were geared to graduated dials. Manual overrides were built in with all the automatic features. The survey total-pressure values were measured on tetrabromoethane manometers and all nine were simultaneously recorded by a remotely controlled K-22 aerial camera located alongside the compressor. All other compressor pressures were recorded with a manually operated camera in the control room on a mercury-manometer board.

#### Accuracy of Data

Runs were repeated on occasion to determine if the data could accurately be reproduced. A typical comparison may be seen on both figures 7(g) and 7(h) after the fifth rotor where the maximum difference in the measured velocity at any point was 2 percent and the average difference

$$\frac{\text{average } \Delta V}{V_{\text{circle}}} 100 = \frac{\int_{\text{hub}}^{\text{tip}} \frac{V_{\text{circle}} - V_{\text{square}}}{V_{\text{circle}}} dr}{r_{\text{hub}} - r_{\text{tip}}} \quad (1)$$

was less than 1 percent. (All symbols are defined in the appendix.)

Although the velocity plots behind a stator row represent only one circumferential position and the ones behind a rotor row are customarily high (because of total-pressure readings usually being high), weight-flow checks of the orifice value were made by assuming the velocities as calculated to be constant circumferentially. Nearly all the runs that were checked agreed within 5 percent.

It might be pointed out that the velocity distribution can have a large error in magnitude, but the boundary-layer parameters will be unchanged if the relative shape is maintained; that is, a proportional increase in  $v$  and  $v_{\text{max}}$  leaves  $\delta^*$  and  $\theta$  essentially unchanged.

#### PROCEDURE

The over-all performance map of the compressor was first made to insure that no peculiarities existed and that the compressor was suitable for the interstage program. Runs were made at speeds from 40 to 100 percent design. Data points were taken at each speed over the range of weight flow from maximum (where the back pressure was the lowest obtainable) to minimum (incipient surge point where the slightest decrease in flow would result in unstable operation, that is, surging). This compressor had a particularly violent surge that produced large amplitude deflections in the outlet piping system and other attachments which were not bolted directly to the bed plate; therefore no surge data were taken.

The aluminum blades of the compressor imposed a temperature limit upon the outlet air because their allowable stress diminished as their temperature exceeded 300° F. Thus the runs were carried out in the following pattern: At speeds of 50 percent of the design speed and lower, room air was used at ambient temperature between 70° and 90° F. At speeds of 60 percent design or above, refrigerated air was used at decreasingly lower temperature until at 100 percent design, air at an inlet temperature no greater than -60° F was required to provide a margin of safety. The stagnation chamber pressure was maintained at 25 inches of mercury absolute during runs at 80 percent design speed or lower and at 15 inches of mercury absolute during runs at 90 and 100 percent design speed. No overspeed runs were made.

## RESULTS AND DISCUSSION

## Over-All Performance

In figure 4 is plotted the over-all pressure ratio against the corrected weight flow with parameters of corrected-percent design speed and adiabatic thermal efficiency. The over-all pressure ratio is the ratio of the total pressure measured in the outlet annulus approximately 1 inch behind the eighth stator row (by the ten-tube rake averages over three radial positions) to the stagnation-chamber total pressure. The corrected weight flow is that value measured by the adjustable orifice, multiplied by the square root of  $\delta$ , and divided by  $\delta$ . The corrected-percent design speed is the actual speed indicated by the chronotachometer instrument divided by the square root of  $\delta$ . The thermal efficiency is calculated with use of the air charts of reference 5 and is

$$\eta_{ad} = \frac{\Delta H_{ad}}{\Delta H_{meas}} \quad (2)$$

with the  $\Delta H$  taken across the entire compressor from the stagnation tank to the instruments after the eighth stator.

As can be seen from figure 4, the weight flow at design pressure ratio fell 3 percent below the design weight flow. The extensive area of peak efficiency (over 80 percent was realized at all speeds shown) indicates good off-design operating characteristics. It is felt that the compromises required to produce specified velocity diagrams entering specified rows handicapped the performance because design velocity diagrams such as shown in figure 7(c) after the fifth rotor, which require a strong radial work input gradient, were not achieved; so succeeding stages suffered. The surge line is smooth except for a slight hump where the weight flow reduced to a very low value at 60 percent design speed, which indicates that any deleterious stage matching effects that may be present must be small. The static-pressure rise through the compressor indicated that the stages were all properly loaded when the compressor was operating at the minimum weight-flow point at each speed. The compressor was satisfactory in range and efficiency for the investigation of interstage losses.

After the compressor had been operated for a total of 255 hours, it was disassembled and examined. Fatigue cracks were found in 18 blades of the first rotor, in 12 blades of the sixth rotor, and in four blades of the sixth stator. Cracks in the first rotor were parallel to the hub, in the center of the chord, and much deeper on the pressure surface than on the suction. The cracks in the sixth stage were ones starting at the small radius fillet, where the after portion of the blade overlapped the blade base, and growing diagonally across the blade. The significance of these cracks will be examined in detail later.

The adiabatic thermal efficiency, with the use of the charts of reference 5, and the static-pressure rise, as measured with the casing static taps, were calculated for each stage throughout the compressor and are shown in figure 5. In the design of this compressor, the axial velocity increases through the first seven stages so that much of the energy added is kept in the kinetic form. Thus for this compressor the static-pressure rise and efficiency would be much lower than the total-pressure efficiency.

Caution must be used in singling out any given stage as bad or good from static-pressure efficiency data because the outlet values of static pressure and temperature of one stage are the inlet values of the next. An inaccuracy in either reading will give a falsely high efficiency in one stage and a falsely low one in its adjoining stage. In the second stage, a 5-percent change in the efficiency will be brought about by an error of either  $0.7^{\circ}$  F or 0.07 inch of mercury at 50 percent design speed and either  $1.6^{\circ}$  F or 0.2 inch of mercury at 100 percent design speed. In the seventh stage, a 5-percent efficiency change is effected by  $1.2^{\circ}$  F or 0.15 inch of mercury at 50 percent design speed and either  $2.5^{\circ}$  F or 0.5 inch of mercury at 100 percent design speed. Some insight into the individual stages is afforded, however. The first stage is seen to be operating inefficiently throughout the weight-flow range at both speeds. At 50 percent design speed, the first stage was undoubtedly operating at a high angle of attack and was stalled, while at 100 percent, mismatching and Mach number effects gave rise to the low efficiency of the stage. Also, subsequent figures of interstage surveys after the guide vanes will show that at some operating conditions the flow is largely tangential or in a negative axial direction at the casing. This is probably a condition induced by tip separation in the first rotor which would have an attendant low efficiency. The second stage (fig. 5) shows complete recovery in nearly all cases because it operates at the average efficiency of the downstream stages. The low back pressure at high weight flows draws air through the latter stages, causing them to turbine and their efficiency to drop to zero. This influence extends as far forward as the fifth stage at 50 percent design speed and to the sixth at 100 percent design speed. The minimum weight-flow curve at 100 percent design speed shows an efficiency in the neighborhood of 80 percent in all stages but the first and sixth. Weight flows between the maximum and minimum values (designated quantities 2 and 3), however, show no unusual drop in the sixth stage. This suggests that the vibrations which cracked the blade in the sixth rotor and stator were present at the minimum weight-flow operating condition and provides a starting point for an investigation into the cracking trouble.

#### Interstage Measurements

The circles on figure 4 indicate the points at which interstage measurements were made. The extensive instrumentation used for the interstage surveys affected the compressor operating characteristics so that these survey points did not lie on the constant-speed lines

determined for the compressor configuration without interstage instrumentation. Surveys of total pressure and flow direction were made behind the guide vanes and behind each blade row from the fifth rotor back at each operating point. Only a few surveys were made in other stages early in the program, but the data from them have been used where applicable. The static pressure on the casing behind each row and the interstage temperature behind each stage were taken from fixed instruments. In calculating the velocity from the data recorded, three assumptions were used: (1) The temperature ahead of a stator row is the same as that measured behind the stator at the same radius. (2) The total pressure indicated by the survey tube in the unsteady flow was the true total (when corrected by the tube's calibration factor) at that position. (3) The static pressure behind a blade row is constant radially at the value that is measured on the casing. The third assumption should introduce errors no greater than would attend a radial static-pressure survey, since the size of a wedge instrument in a small channel will affect its readings. Radial static-pressure variations may be expected in stages with low hub-tip ratios or in stages with high tangential velocities. A check was made of the velocity distribution behind the inlet guide vanes at each operating point calculated by the method of reference 7, which includes the radial static-pressure change due to the radial distribution of the tangential velocity as determined from the simple radial equilibrium condition. The absolute velocity behind the guide vanes at radius  $r$  is given by

$$V = V_{\text{ref}} \exp\left(\int_r^{r_{\text{ref}}} \sin^2 \beta \frac{dr}{r}\right) \quad (3)$$

The reference velocity  $V_{\text{ref}}$  was taken as that at approximately the mid-channel survey point. As can be seen in the guide-vane plots of figures 6 and 7, very small differences are produced by assuming the change of static pressure with respect to the radius to be zero. This results from the extremely low absolute tangential velocities after the guide vanes.

A further check of the calculated velocity distribution was made after the sixth rotor (figs. 7(g) and 7(h)) and after the eighth rotor (figs. 7(e) and 7(f)) where the tangential velocities are high. As a velocity check in these blade rows, use was made of the method of reference 7 for calculating velocities at a station having a radial variation in enthalpy, with simple radial equilibrium assumed. The method of reference 7 was modified for the present application by consideration of the effects on the velocities of varying entropy along the radius. The small differences between the two calculated results indicate that the assumption of constant static pressure can be considered valid in the present case.

The velocity is presented in its axial and tangential components. Figure 6 shows the four 50-percent-speed runs and figure 7 the four 100-percent runs. In instances where the data were incomplete or its reliability suspected, the curves were estimated as accurately as possible and drawn with dashed lines.

The great majority of the profiles are similar to a turbulent channel-flow profile, increasing monotonically from the walls to the free stream. Some, however, reveal multiple velocity peaks, areas of seemingly great boundary layer, or even separated flow. These unusual effects appear almost exclusively behind stator rows and may be ascribed to one or more of three things: (1) upstream disturbances such as the wake from a blade in the preceding stator row; (2) the artificial scheme of resolving the flow velocity into axial and tangential components which have no relation with the direction of the viscous forces and thus create peculiar views of the flow pattern or false illusions of separation; (3) the limitations of one circumferential surveying position. The false impression and the circumferential limitations are very apparent in the velocity pictures behind the guide vanes in figures 6(a) and 6(b). The axial velocity has a separation profile at the casing and there seems to be no net through flow. The tangential-velocity plot, however, reveals that the air is not separated, only that it is traveling primarily in a circumferential direction at the casing with a slightly negative axial component. Because there is considerable through flow, it must be passing at other circumferential positions, probably nearer the pressure surface of the adjacent vane than the surveying station.

In figures 8 and 9 the boundary-layer-thickness parameters from the axial-velocity profiles are plotted to show the variation through the compressor. The regions classically designated as boundary layer are those in which the viscous forces predominate over the inertia forces, but the smooth rounding of these velocity profiles from the latter stages makes it unreasonable to pick a definite point as the termination of the steep  $\partial v_a / \partial r$  gradient. Therefore the viscous effect was assumed to extend from the wall to the radial point of maximum velocity  $r_v$  in each case. For example, on the axial-velocity plot after the fifth stage in figure 6(a), the point at  $r = 6.53$  was taken as the maximum. The curve was extrapolated to the hub and the areas indicated by cross hatching were considered as the loss in velocity from viscous action. This criterion was used throughout in the absence of a more reasonable one that could be universally applied. Irregular curves for which this criterion could not be used, such as after the eighth stator in figure 6(a), where the velocities at the edge of the boundary layers on the hub and casing reached different maximum values at  $r = 6.61$  and  $r = 6.92$ , respectively, were calculated in a manner as consistent as possible with the criterion. It must be borne in mind, throughout the remainder of the data, that the losses indicated by the values of the boundary-layer parameters thus obtained will, in most instances, be numerically larger than may rightly be attributed to the boundary layer.

The values of the displacement thickness

$$\delta_a^* = \frac{1}{v_{a,\max}} \int_{r_{\text{wall}}}^{r_v} (v_{a,\max} - v_a) dr \quad (4)$$

and the momentum thickness

$$\theta_a = \frac{1}{(v_{a,max})^2} \int_{r_{wall}}^{r_v} v_a (v_{a,max} - v_a) dr \quad (5)$$

were obtained by graphical methods with a planimeter.

Figures 8 and 9 show the displacement thickness to vary much more in magnitude than the momentum thickness. At low weight flows the boundary layer on the casing is large behind each rotor row and small behind each stator row almost without exception. The hub boundary layer has the opposite variation. Thus, behind a blade tip (having a clearance space) the boundary layer is proportionately large and behind a blade base (which is attached) the boundary layer is proportionally small. In table I the running clearance is given as 0.018 inch or less, which is roughly  $1\frac{1}{2}$  percent of the passage after the fifth rotor and 3 percent of the passage after the eighth stator. This is the same order of magnitude as the boundary-layer thickness in many locations. With the continuously positive pressure gradients at low weight flow, the magnitude of the total thickness increases through the latter stages. As the pressure gradients decrease at higher weight flows, the boundary-layer values show less fluctuation and the magnitude becomes relatively constant or even diminishes through the latter stages.

The two parts of figure 10 show that the magnitude of the momentum thickness in the latter stages at 100 percent design speed is practically the same as at 50 percent design speed. Figure 10(a) presents the maximum size of the momentum thickness appearing in the latter stages. It is labeled the reasonable maximum because the two or three largest values are considered rather than the greatest one only so that a single, isolated, extreme value will not have undue importance. Figure 10(b) is the arithmetic average of the total momentum-thickness values in the last four stages.

The sixth stage has erratic boundary-layer values at some of the conditions tested, especially at 100 percent design speed. Table I shows that the blades at the hub of the sixth rotor have a greater design turning angle than any other blades in the compressor and practically  $2^\circ$  more than any other blades in the rear four stages. The sixth stage might logically be expected to develop a rotating stall in the rotor before any other rear stage would (reference 8). This, of course, affects its stator, the interstage pressures measured, and hence the velocity, boundary-layer values, and efficiency characteristics calculated. When the compressor was disassembled and examined after the program was completed, this was the only stage (except the first rotor) that had fatigue-cracked blades (see Over-All Performance section). A vibration was obviously present in this stage that was not in the other rear stages. The erratic boundary-layer values might well be expected from vibrating surfaces of a blade driven by an unsteady exciting force

and the rotating stalls themselves. The design turning angle, which is greater-than  $27^\circ$ , evidently did not allow sufficient margin for the greater-than-design angles of attack that are produced by overturning in the wall boundary-layer regions and by off-design operation.

### ANALYSIS

It is seen in figures 6 and 7 that the axial velocity profiles in the latter stages are not sharply peaked at midpassage similar to Poiseuille flow, as has been indicated by past investigations (references 1 and 2). In order to understand the flow pattern that exists, the flow mechanisms present in a turbomachine must be studied. The motions that are imposed upon the through flow can be individually considered and then their combined effects can be grasped more clearly.

It is recognized that the air flow at any point in a compressor is nonsteady in stator rows as well as rotor. This is due to the wakes and the variations in flow velocity that exist from the suction-to-pressure surface of the upstream row of blades which are moving tangentially with respect to the point. Although an airfoil behaves differently in fluctuating flow than in steady flow, the effects of changing angle of attack, increasing and decreasing circulation, and so forth, are damped in each stage and are recorded by a pressure tube immersed in the stream as steady flow at some averaged value. From the aerodynamics of unsteady motion it is known that a variation of circulation with time leads to the shedding of free vortices from the trailing edge, the kinetic energy of which must be considered as a loss except for the benefit of its mixing effect. The action of turbulence in a stream is incompletely understood aside from its tendency to make the flow energy homogeneous throughout. The high turbulence level in a compressor is an asset in that it readily disperses surface friction effects throughout the flow by an interparticle exchange of energy. This might be thought of as a minor macroscopic motion in the sense that it is local in its scale and effect.

### Flows Imposed upon Through Flow

Motions which might be called major macroscopic motions are impressed upon the through flow and these motions will usually be present under steady or unsteady conditions with little or much turbulence. It is these motions that transport particles of air that have been retarded by friction along the annular walls into the main flow, thereby decreasing their rate of build-up under the large positive pressure gradients encountered. These may be separated into categories of local pressure deflection (so-called secondary flow), tip-clearance flow, and motion due to irrotationality. The moment of momentum balance, in addition, indicates the radial forces that particles with depleted momentum will

experience, hence their radial motion. The unsteady properties of the flow will not be examined further. The approximately root-mean-square averaged values recorded from the pressure tubes will be considered the steady condition as the large macroscopic motions are examined.

Secondary flow. - By secondary flow is meant the flow motions of the viscously retarded fluid particles, adjacent to the annular surfaces, that are induced by the pressure field produced in a curved blade passage. This motion is illustrated in figure 11.

This secondary flow has been explored by many authors. Reference 9 follows the blade vorticity approach and presents a qualitative discussion of the general nature of secondary flows within the passages of stationary annular cascades for the through-flow regions as well as the end-wall boundary-layer regions. Quantitative evaluation of the radial variation of the actual mean flow caused by the wall boundary layers was successfully obtained by using a distribution of vorticity related to the blade design superimposed on the ideal blade-element flow of the cascade. An empirical factor was developed to correlate theoretical and experimental results.

The approach that uses the fluid vorticity distribution at the inlet and the action of forces within the channel has been used with success in references 10 and 11. Reference 10 deals with two-dimensional, steady, incompressible, viscous flow to describe small-scale secondary effects. By assuming a reasonable velocity distribution and friction law for the turbulent boundary layer, solutions for the momentum thickness and the direction of the deflected flows in the boundary layer are obtained. This has been directly applied to an axial-flow compressor (reference 12) and shown to be useful in predicting some viscous deflections of the main flow. The component of the low-momentum flow which is perpendicular to the main flow is useless energy, but it is demonstrated that succeeding stages with their alternating curvature induce a redirection of some of this energy into a utilizable direction. Reference 11 treats the steady, incompressible, inviscid case and applies it to duct bends by considering the component of vorticity in the flow field which is aligned with the velocity vector. A relation is shown between the change of this vorticity component and the velocity, streamline curvature, and total-pressure gradient. Also, that more than one stable flow pattern can result from a given inlet condition is shown to be possible.

Tip-clearance flow. - The values of the boundary-layer parameters in figures 8 and 9 are almost, without exception, much larger behind the unattached tips of the blades than behind the attached roots of the blades. This is true of both the rotors and the stators.

Tip-clearance flow is the product of the pressure difference which exists between the pressure and suction side of a blade (as on a wing) and the viscous forces of the annular wall (which has a velocity relative to the blade). The studies of reference 13 reveal the nature of the flow (which is imposed upon the through flow) to be as sketched in figures 12 and 13. When there is no relative motion between the blades and the wall, the investigation of reference 13 for the same type of blading as that used in the compressor reveals that the tip-clearance vortex is approximately of the same order of magnitude as the secondary flow across the passage. These opposing fields prevent fanning out of the tip flow into the passage, so that it rolls into a tight, rapidly rotating vortex in the suction-surface corner, as pictured in figure 12. The secondary flow is deflected around the vortex with no apparent mixing. With a relative motion between the blades and the wall, the flow entrained by the viscous action of the wall is of a much greater order of magnitude than the secondary flow and largely obliterates it. The aspirating effect at the trailing-blade surface (cf. reference 13) even draws flow on the suction surface toward the tip. The viscous region at the leading-blade surface is highly turbulent and extends perpendicular to the wall a distance many times the magnitude of the clearance. A much larger quantity of air is deflected tangentially than can pass beneath the adjacent blade tip so that it is rolled up in the pressure-surface corner, as shown in figure 13. Because of this tangentially deflected flow and the energy tied up in turbulent eddies, a pressure probe surveying at the midchannel position will see particles with less axial momentum when in a blade tip region than in a blade base region. This result will be accentuated by the effects of radial pressure gradients and centrifugal action on the boundary-layer particles.

Figure 10 shows the magnitude of the losses at 100 percent design speed to be practically the same as at 50 percent. An examination of the factors that control the tip-clearance flow reveals that, as the speed is increased, the viscous forces increase as the first power of the tip speed; the blade loading rises, increasing the pressure forces (which affects the clearance flow as the 0.286 power of the pressure ratio); but the blade is stretched and the clearance area is decreased as the square of the tip speed. It appears that these effects in conjunction with the centrifugal-force effects and the radial pressure gradients attained some sort of balance which kept losses relatively constant for the conditions of 50 and 100 percent design speed.

Past evaluations of tip loss that have been published were on single-stage units, and the results were presented as gross effects in terms of a decrease in stage efficiency or work. Since the losses are appreciably greater at the free end of blades than at their attached end, the tip-clearance flow contributes to the viscous diminishing of the downstream velocity which affects succeeding stages. This veiled influence makes the efficiency loss in a multistage greater than in a single-stage machine. References 14 and 15 are two early tip-clearance investigations. In reference 14 a theoretical analysis is made but

found to agree poorly with the experimental data. Reference 15 presents the effect of tip clearance on efficiency and the surge line in a single-stage compressor. It was concluded, with the assumption that the efficiency is a linear function of the clearance in the range

$0.002 \leq \frac{c}{2R} \leq 0.012$  investigated, that for the commonly used value

$\left(\frac{c}{2R} = 0.002\right)$  there is a reduction in efficiency of 2 to 3 percent.

Reference 16 examines flow details in a turbine and presents a theory that agreed well with experimental results. It was found that the losses at the tip due to clearance flow were 3 times the losses due to all other causes, for example, secondary-flow vorticity. However, the range of  $c/l$  considered was from 1.5 to 8 times as great as the extreme in the eight-stage compressor herein. Also, the opposing pressure and viscous forces across a turbine blade tip make it necessary to modify any application to a compressor. Reference 17 sums up the gross effect of compressor tip clearance as producing a reduction in efficiency of 1.5 to 2.5 times  $c/h$ . Some approximate calculations are quoted that show one third of the loss at the free end of the blade to be attributed to the reduction in blade height and the remainder to induced flow. Also results of varying tip clearance in multistage compressors are quoted which suggested that losses per stage are less than for a single stage. This conclusion, undoubtedly, did not consider the veiled influence upon downstream stages, discussed previously, as a part of the clearance loss. Reference 18 analyzes the flow on a volumetric efficiency basis but does not consider the change in clearance with blade speed. The data show that doubling the clearance at design speed drops the efficiency 3 to 4 percent. However, only one thermocouple located at the mean blade height was used to calculate the efficiency.

All but reference 16 consider the gross effect of tip clearance upon efficiency. Until a more complete understanding is achieved, all indications are that it is advisable to keep running clearances small.

Motion due to irrotationality. - In accord with Newton's first law, fluid which has no rotation (with respect to absolute coordinates) that passes into a rotor will have a rotation relative to the rotor and opposite in sense to the rotor rotation. This characteristic of a fluid to maintain its absolute orientation is its irrotationality. A real fluid will maintain only partial irrotationality because viscous action opposing the relative rotation in a rotor imparts small absolute rotation in the rotor direction to the fluid which it will carry, by Newton's first law, into the following stator. Hence in each blade row after the guide vanes there will be a rotation of the fluid relative to the blades. This is illustrated in figure 14. Because the fluid is without rotation initially, the magnitude of the motion will be much greater in a rotor row than in a stator row. Each stator will act as a damper although

less rotation can be damped out in a stator than is imparted in a rotor because the relative motion is less. In all rotors and in the stators of the latter stages (where the accumulated absolute rotation will be of sizable magnitude) this must be considered as a major macroscopic motion.

If an average air velocity of 600 feet per second (from figs. 6(g) and 6(h)) at 50 percent of design speed is assumed, it will take  $1.4 \times 10^{-4}$  seconds to pass through a rotor blade passage having 1.013-inch chord (from table I) and the passage will rotate through  $6.4^\circ$  in that length of time. An average air velocity of 700 feet per second (from figs. 6(g) and 6(h)) at 100 percent design speed will take  $1.2 \times 10^{-4}$  seconds to pass through and the passage will rotate through  $11^\circ$  in that length of time. Thus the flow from a stator row including the depleted wake and wall losses it carries is rotated in the rotor row and enters the following stator skewed. Likewise the absolute rotation that the rotor has given the fluid will skew the rotor wakes and wall losses as they pass through the stator row. This rotational motion acts, therefore, as do the other macroscopic motions, to transport low-momentum regions away from the surfaces upon which they can build up.

#### Moment of Momentum Stability

For air flowing over a surface that is at a different temperature from the air, it is easily seen how the body forces that are changed by the heat transferred will produce a stable boundary layer on a surface colder than the air and an unstable boundary layer on a hotter surface. Similarly, for air flowing between two concentric rotating cylinders, the stability controlling factor of major importance is the balance between the inertia and pressure forces. This equation of motion

$$\frac{dv_r}{dt} = \frac{v_t^2}{r} - \frac{1}{\rho} \frac{\partial p}{\partial r} = \frac{(rv_t)^2}{r^3} - \frac{1}{\rho} \frac{\partial p}{\partial r} \quad (6)$$

where  $rv_t$  is the moment of momentum, shows that the unsteady velocity in the radial direction is determined by the centrifugal force and pressure gradient.

A solution of the complete stability problem considering the pressure, inertia, and viscous forces in unsteady flow is given in reference 19. Instability within the channel is analyzed as a function of the rotative speeds of the hub and the casing. This compressor has a stationary casing and rotating hub which is shown to have an instability level lower than any other combination and would be the most favorable boundary-layer wise. The flow pattern is, of course, greatly changed by the blades and through flow.

This stability has been applied to turbomachinery in reference 20. A particle will retain its initial moment of momentum  $rv_t$ , by the law of conservation of momentum, when displaced to a position where a different moment of momentum  $(rv_t)_d$  exists. A restoring force, proportional to the difference, will be felt by the particle if the existing moment of momentum is less than  $rv_t$  and an accelerating one if it is greater

$$\text{force} = \frac{\rho_d (rv_t)_d^2}{r_d^3} - \frac{\rho (rv_t)^2}{r_d^3} \quad (7)$$

or, with the density change neglected,

$$\text{force} = K(rv_t)_{av} \left[ (rv_t)_d - (rv_t) \right] \quad (8)$$

where the proportionality constant  $K$  is equal to  $2\rho/r_d^3$  and  $(rv_t)_{av}$  is the average moment of momentum.

The rotating hub and the stationary casing have little effect upon the pressure field because it is imposed by the main body of flow. At the hub the air particles have the tangential velocity of the hub which is much greater than that of the main stream air (figs. 6 and 7), so that the centrifugal force upon them is greater than the imposed pressure gradient and a displacement moves them farther away from the hub. Moving particles at the casing are slowed by viscosity so that they have less centrifugal force than the main stream air and will be moved away from the casing. Since this resistance to low-momentum particles accumulating on the annular walls is present, blade wakes will remain in the main body of flow to be dissipated, making no contribution to the boundary-layer build-up but diminishing the average main flow velocity.

#### Modification of Velocity Profiles in Latter Stages by Viscosity

The minimum-weight-flow curve of figure 8 shows a gradual increase in the total values of the boundary-layer parameters through the seventh stage, then a rapid decrease through the eighth. The low-weight-flow curves of figure 9 are similar; the increase is proportionately greater and the drop off is more severe. As can be seen from figure 7(c), the design values of the axial velocity increase through the seventh stage then decrease through the eighth. Comparison of design values and actual values show that the boundary layer does not continuously build up, as has been considered in the past, to produce a pronounced velocity

peak at midpassage. Rather, the macroscopic motions have produced a mixing of the depleted air with the main stream flow to make the whole of the main stream velocity more uniform. The behavior of low-momentum fluid particles seems to be as follows: Low-energy fluid near an annular wall is moved across the passage, up a blade, and into the blade wake where it is mixed with the main flow. The boundary layer measured behind the attached end of a row of blades is relatively new because it has flowed over only a short friction surface, that is, down a portion of the blade and across a small annular surface distance. The boundary layer behind the free end of a row of blades is increased by the clearance flow. The tip-clearance vorticity that opposes the secondary motion moves low-momentum fluid away from the annular boundaries. The clearance flow is not necessarily of low momentum (it may be high), but it requires redirecting, which the following stage does to a limited degree. High vortical velocities of some imposed flows (secondary, tip) create low-static-pressure regions into which low-momentum air will be drawn and a core of low-energy air exists which the subsequent row moves into the free stream to be dissipated.

The eight-stage compressor of this investigation had an increasing axial velocity through most of the stages, which is not a common condition in present commercial compressors. Increasing axial velocity is possibly more favorable boundary-layer wise because the increase of energy is kept in a kinetic form and is a restriction upon the generality in interpreting these results. The stage static-pressure rise, which is the principal factor, is thus kept less than the stage total-pressure rise but still has a significantly large value because the total-pressure rise was 1.23, much larger than practically all commercial compressors.

Choking tendencies in the rear stages, as have been found in some compressors, were not found in this compressor. One compressor which exhibits choking tendencies in the ninth to the twelfth stages was designed with a 0.6 Mach number limit, and the combination of stage pressure and temperature rise gave an increasing axial velocity throughout. It was designed by using an efficiency factor and then opening the area 10 percent throughout; this area increase may have been too much in the early stages and too little in the latter, which would result in poor stage matching. It has extremely small blades (0.40 in. high by 0.429 in. chord in the twelfth stage) and high hub-tip ratios  $\left(\frac{r_{\text{hub}}}{R} > 0.9\right)$  in the last four stages with a twelfth stator value of 0.952 with a 1.20 stage total-pressure ratio. As a comparison, the eighth (final) stator blade of the compressor investigated herein had a height of 0.58 inch, a chord of 1.013 inches, a radius ratio  $\frac{r_{\text{hub}}}{R} = 0.924$ , a

decreasing design axial velocity, and a design stage total-pressure ratio of 1.23. There seems to be a lower limit to the physical dimensions permissible that was exceeded by one and not by the other compressor. The compressor of reference 21 was designed by a method very similar to that of the preceding twelfth-stage compressor, and its performance was outstanding. The increased physical scale must have sufficiently separated the high-loss regions at the blade ends to permit the dispersion and absorption of low-energy particles in the main flow.

The use of suction on the walls of the annular passage of the later stages has often been contemplated. The phenomena observed in this investigation permit some conclusions to be drawn on the advisability of using suction. The fluid motions that bring higher-energy fluid to the annular surfaces in alternating blade rows effectively reenergize the boundary region and diminish the area blocked (the displacement thickness). This makes the use of suction in a properly designed compressor unpromising. A compressor from which it is necessary to bleed air for turbine cooling, accessory operation, and so forth, could remove the air from such a location (probably over the rotor tips) that the lowest-energy fluid is taken and the flow aerodynamics would be aided. An existing compressor with choking difficulties might be improved by suction. Of itself, however, suction appears to offer little gain at a large cost in additional apparatus.

#### Design Compensation for Viscosity

Since the action of viscosity is to decrease the weight flow, a design must include an enlargement of the flow area in order that the desired weight flow will be passed. At the present status of the art, this is handled as a gross effect in the design. The use of both an efficiency factor and an arbitrary increase of the flow area has the same effect as using a lower efficiency without increasing the flow area. There are three schemes designers commonly employ to compensate for viscosity: A "work done" factor, as described in reference 16, can be applied. A conservative efficiency value can be taken which will give a relatively large amount of area increase. Or a high value of efficiency can be used, with the assumption that the calculations apply to the main flow, and then the area can be increased proportionately as assumed boundary-layer parameters indicate is necessary. The polytropic efficiency used to calculate pressure ratio (and consequently area ratio) from the temperature rise will show a greater area correction for a design having a high stage pressure ratio. Also, as Mach numbers above approximately 0.55 are used, the rate of change of weight flow with efficiency increases greatly as the Mach number increases. Thus, the choice of efficiency becomes critical as high stage pressure ratios and Mach numbers are utilized.

## CONCLUSIONS

The following conclusions are drawn about the action of viscosity in the latter stages of a multistage axial-flow compressor having a design similar to the compressor reported herein:

1. The fluid retarded by viscous action does not accumulate primarily along the annular surfaces but is mixed into the main body of flow by distinct macroscopic motions that are imposed upon the main flow. Velocity profiles do not exhibit pronounced peaks such as in pipe flow.
2. The annular wall boundary layers, as measured by a single radial survey at midchannel, are small behind blade roots because the secondary flow motion has swept away the entering boundary layer and carried a small boundary layer down off the pressure side of the adjacent blade. They are large behind blade tips since the roll up of flow on the leading-blade surface is accentuated by the effects of radial pressure gradients and centrifugal action on the boundary-layer particles.
3. An intermediate stage can have an unusually large boundary layer in the axial direction and still be highly efficient.
4. The maximum values of the boundary-layer parameters increase as the weight flow decreases, that is, the static-pressure gradient increases, at a given speed.
5. At high weight flows the annulus wall boundary layers remain relatively constant in magnitude or diminish through the compressor. At low weight flows their magnitude increases through the compressor.
6. There is a lower limit to the physical blade size that can be used in the latter stages of an axial-flow compressor. The macroscopic mixing motions cannot prevent choking in blades that are too small.

Lewis Flight Propulsion Laboratory  
National Advisory Committee for Aeronautics  
Cleveland, Ohio

## APPENDIX - SYMBOLS

The following symbols are used in this report:

c	tip clearance, ft
H	enthalpy corresponding to stagnation condition, Btu/lb
h	blade height, ft
K	proportionality constant
l	blade chord, ft
N	compressor speed, rpm
P	total pressure, lb/sq ft abs
p	static pressure, lb/sq ft abs
R	casing inside radius, 0.583 ft (7 in.)
r	radius, ft
$r_v$	radius at which maximum velocity occurs, ft
t	time, sec
V	absolute velocity, ft/sec
v	velocity component, ft/sec
$v_e$	equivalent tangential velocity of hub $\left(2\pi r_{\text{hub}} \frac{N}{60 \sqrt{\delta}}\right)$ , ft/sec
W	weight flow, lb/sec
y	coordinate perpendicular to the surface
$\beta$	angle between absolute velocity direction and axial direction, deg
$\delta$	ratio of stagnation chamber total pressure to NACA standard sea-level pressure (14.696 lb/sq in.)
$\delta^*$	boundary-layer displacement thickness, ft
$\delta_T$	total boundary-layer thickness

$\eta$  efficiency  
 $\theta$  boundary-layer momentum thickness, ft  
 $\delta$  ratio of stagnation chamber total temperature to NACA standard sea-level temperature (518.6 °R)  
 $\rho$  density, slugs/cu ft

## Subscripts:

a axial  
ad adiabatic thermal  
av average  
d displaced  
max maximum  
meas measured  
min minimum  
r radial  
ref reference  
t tangential

## REFERENCES

1. Ainley, D. G., and Jeffs, R. A.: Analysis of the Air Flow through Four Stages of Half-Vortex Blading in an Axial Compressor. R. & M. No. 2383, April 1946.
2. Bowen, John T., Sabersky, Rolf H., and Rannie, W. Duncan: Theoretical and Experimental Investigations of Axial Flow Compressors. Pt. 2. Mech. Eng. Lab., C.I.T., July 1949. (Navy Contract N6-ORI-102, Task Order IV.)
3. Sinnette, John T., Jr., Schey, Oscar W., and King, J. Austin: Performance of NACA Eight-Stage Axial-Flow Compressor Designed on the Basis of Airfoil Theory. NACA Rep. 758, 1943. (Supersedes NACA ACR E4H18.)
4. Bogdonoff, Seymour M., and Bogdonoff, Harriet E.: Blade Design Data for Axial-Flow Fans and Compressors. NACA ACR L5FO7a, 1945.
5. NACA Subcommittee on Compressors: Standard Procedures for Rating and Testing Multistage Axial-Flow Compressors. NACA TN 1138, 1946.
6. Finger, Harold B., and Dugan, James F., Jr.: Analysis of Stage Matching and Off-Design Performance of Multistage Axial-Flow Compressors. NACA RM E52D07, 1952.
7. Finger, Harold B.: Method of Experimentally Determining Radial Distributions of Velocity Through Axial-Flow Compressor. NACA TN 2059, 1950.
8. Huppert, Merle C.: Preliminary Investigation of Flow Fluctuations During Surge and Blade Row Stall in Axial-Flow Compressors. NACA RM E52E28, 1952.
9. Lieblein, Seymour, and Ackley, Richard H.: Secondary Flows in Annular Cascades and Effects on Flow in Inlet Guide Vanes. NACA RM E51G27, 1951.
10. Mager, Artur: Generalization of Boundary-Layer Momentum-Integral Equations to Three-Dimensional Flows Including Those of Rotating System. NACA Rep. 1067, 1952. (Supersedes NACA TN 2310.)
11. Eichenberger, Hans P.: Shear Flow in Bends. Tech. Rep. No. 2, Office Naval Res., Gas Turbine Lab., M.I.T., April 15, 1952. (Contract N5 ori 07848.)
12. Mager, Artur, Mahoney, John J., and Budinger, Ray E.: Discussion of Boundary-Layer Behavior Near the Casing of an Axial-Flow Compressor. NACA RM E51H07, 1951.

13. Hansen, A. G., Costello, G. R., and Herzig, H. Z.: Effects of Geometry on Secondary Flows in Blade Rows. NACA RM E52H26, 1952.
14. Sédille, Marcel: The Effect of Clearance on Axial Compressors. Comptes Rendus, vol. 208, Jan.-March, 1939, pp. 418-420.
15. Ruden, P.: Investigation of Single Stage Axial Fans. NACA TM 1062, 1944.
16. Meldahl, A.: End Losses of Turbine Blades. Jour. Am. Soc. Naval Eng., vol. 54, no. 3, Aug. 1942, pp. 454-466.
17. Howell, A. R.: The Present Basis of Axial Flow Compressor Design. Part II. Compressor Theory and Performance. Rep. No. E. 3961, R.A.E., Dec. 1942.
18. Fickert: The Influence of the Radial Clearance of the Rotor on the Compressor Efficiency, Dec. 12, 1944. Part C of the Influence of Physical Dimensions (Such as Hub:Tip Ratio, Clearance, Blade Shape) and Flow Conditions (Such as Reynolds Number and Mach Number) on Compressor Characteristics. Buships 338, Navy Dept., May 1946, pp. 95-108.
19. Taylor, G. I.: Stability of a Viscous Liquid Contained Between Two Rotating Cylinders. Phil. Trans. Roy. Soc. (London), ser. A, vol. 223, 1923, pp. 298-343.
20. Goldstein, Arthur W.: Analysis of Performance of a Jet Engine from Characteristics of Components. I - Aerodynamic and Matching Characteristics of Turbine Component Determined with Cold Air. NACA Rep. 878, 1947. (Supersedes NACA TN 1459.)
21. Budinger, Ray E., and Thomson, Arthur R.: Investigation of NACA 10-Stage Subsonic Axial-Flow Compressor. II - Preliminary Analysis of Over-All Performance. NACA RM E52C04, 1952.

TABLE I - COMPRESSOR DESIGN DATA

Stage	Angle between compressor axis and blade chord line		Number of blades	Blade height (along blade axis) (in.)	Blade chord (in.)	Blade tip clearance (in.)		Blade profile	Turning angle (deg)	
	Casing	Hub				Stationary clearance	Calculated running clearance		Casing radius	Hub radius
Guide vane	A tangent to the leading edge is parallel to compressor axis		35	3.31	Hub, 1.157 Tip 2.000	0.012	0.015	Circular arc, 3.372 in. radius	17.25	9.88
1st rotor	65°45'	33°33'	22	2.76	1.310	0.025	0.018	65-(12)10	6.15	22.45
1st stator	37°12'	29°45'	25	2.46	1.310	.022	.018	65-(12)10	12.91	18.83
2nd rotor	61°30'	30°30'	26	2.20	1.310	.028	.018	65-(12)10	8.74	25.47
2nd stator	39°48'	30°18'	27	1.96	1.310	.025	.018	65-(12)10	13.74	21.78
3rd rotor	53°48'	25°12'	28	1.73	1.310	.030	.017	65-(12)10	12.43	26.02
3rd stator	36°12'	28°54'	29	1.52	1.310	.026	.017	65-(12)10	18.42	23.34
4th rotor	47°51'	26°20'	30	1.34	1.310	.033	.017	65-(12)10	12.98	25.34
4th stator	32°55'	27°33'54"	42	1.18	1.013	.030	.017	65-(12)10	19.87	24.18
5th rotor	38°02'	25°44'	43	1.05	1.013	.036	.017	65-(12)10	21.52	25.09
5th stator	29°11'	30°45'	44	.96	1.013	.031	.017	65-(12)10	24.19	22.59
6th rotor	34°30'	24°30'	45	.85	1.013	.039	.017	65-(12)10	21.05	27.15
6th stator	29°37'	29°37'	44	.77	1.013	.032	.017	65-(12)10	23.02	24.32
7th rotor	30°44'	25°39'	45	.66	1.013	.040	.016	65-(12)10	21.90	25.35
7th stator	30°0'	30°0'	46	.61	1.013	.033	.016	65-(12)10	21.80	23.07
8th rotor	28°30'	28°30'	47	.54	1.013	.040	.015	65-(12)10	22.63	23.74
8th stator	28°30'	28°30'	48	.55	1.013	.035	.015	65-(12)10	23.92	25.17

Axial distance from leading-edge guide vanes to trailing-edge 8th stator, 22 in.

Rotor blade tip diameter, 14.00 in.

Angles of blades varied linearly from hub to tip

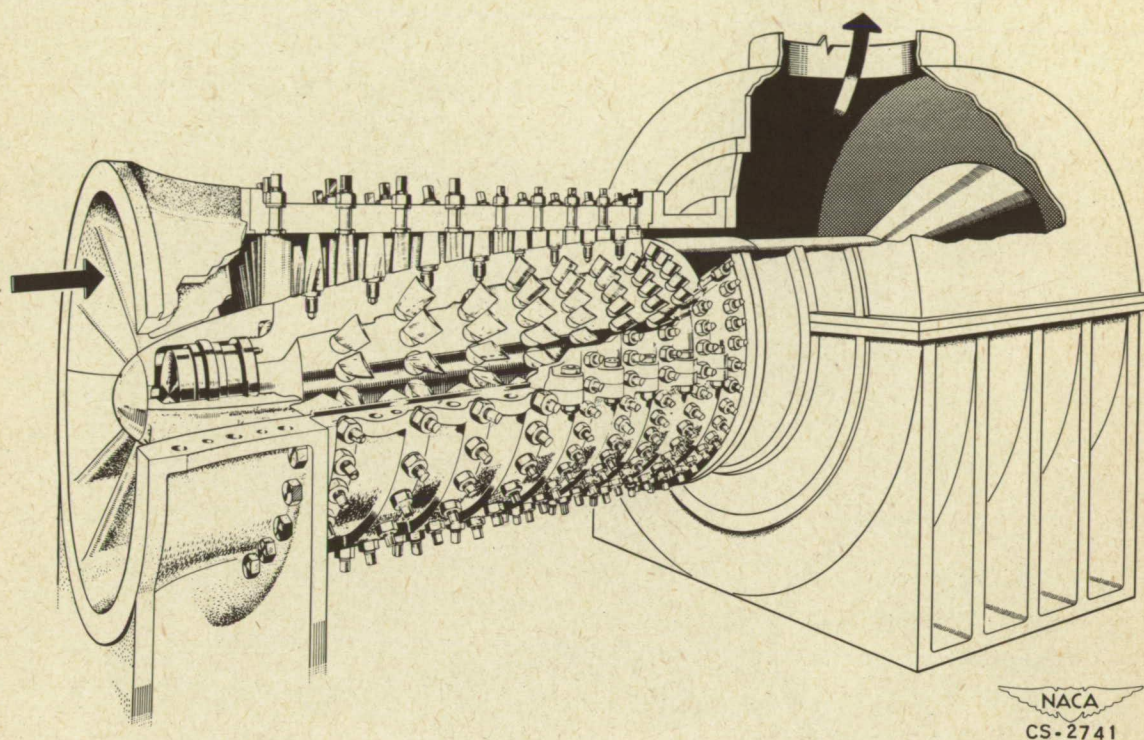


Figure 1. - NACA eight-stage axial-flow compressor with collector.

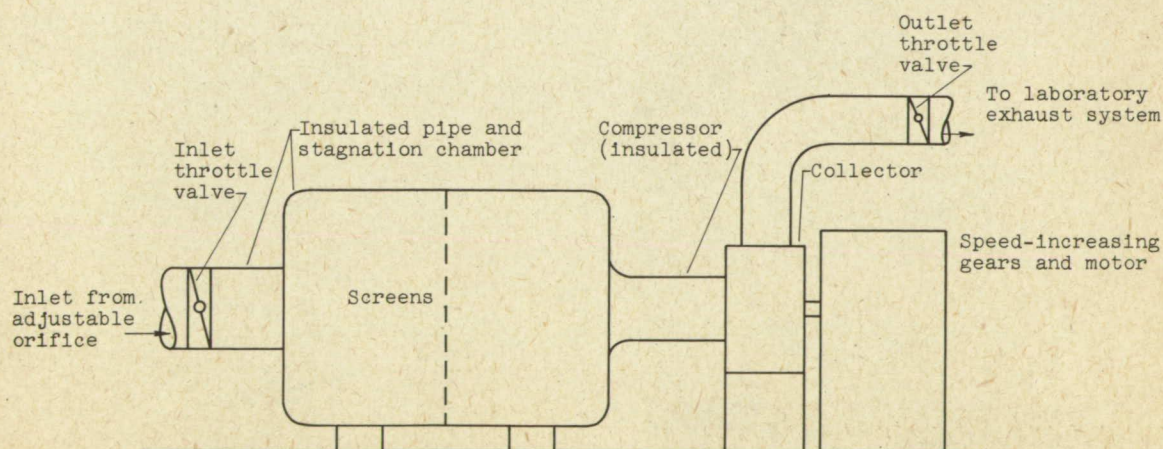


Figure 2. - Schematic diagram of compressor testing arrangement.

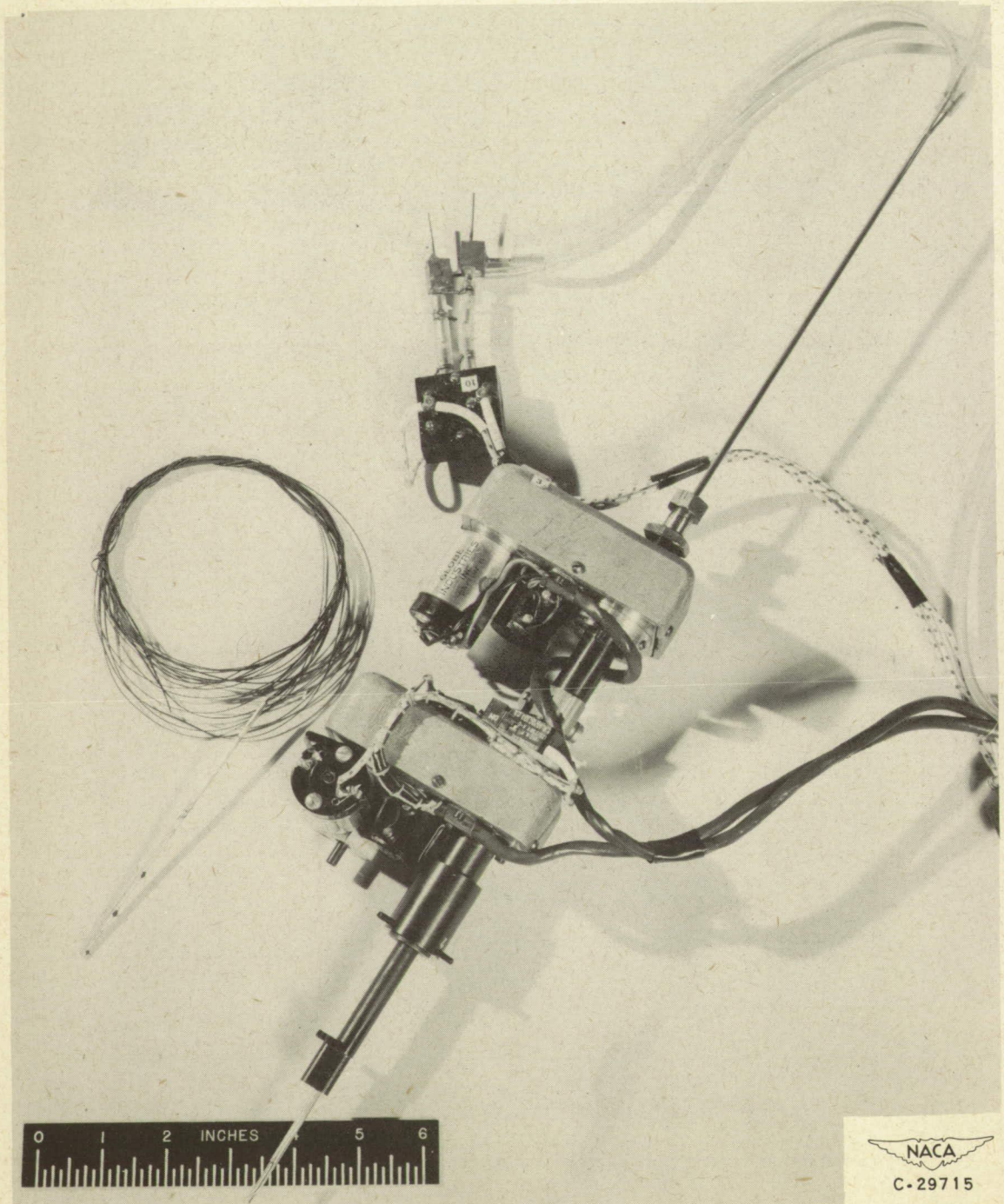


Figure 3. - Three-spike thermocouple rake and instrument actuator having 1/8-inch-diameter claw total tube and automatic angle-balancing capsule mounted.

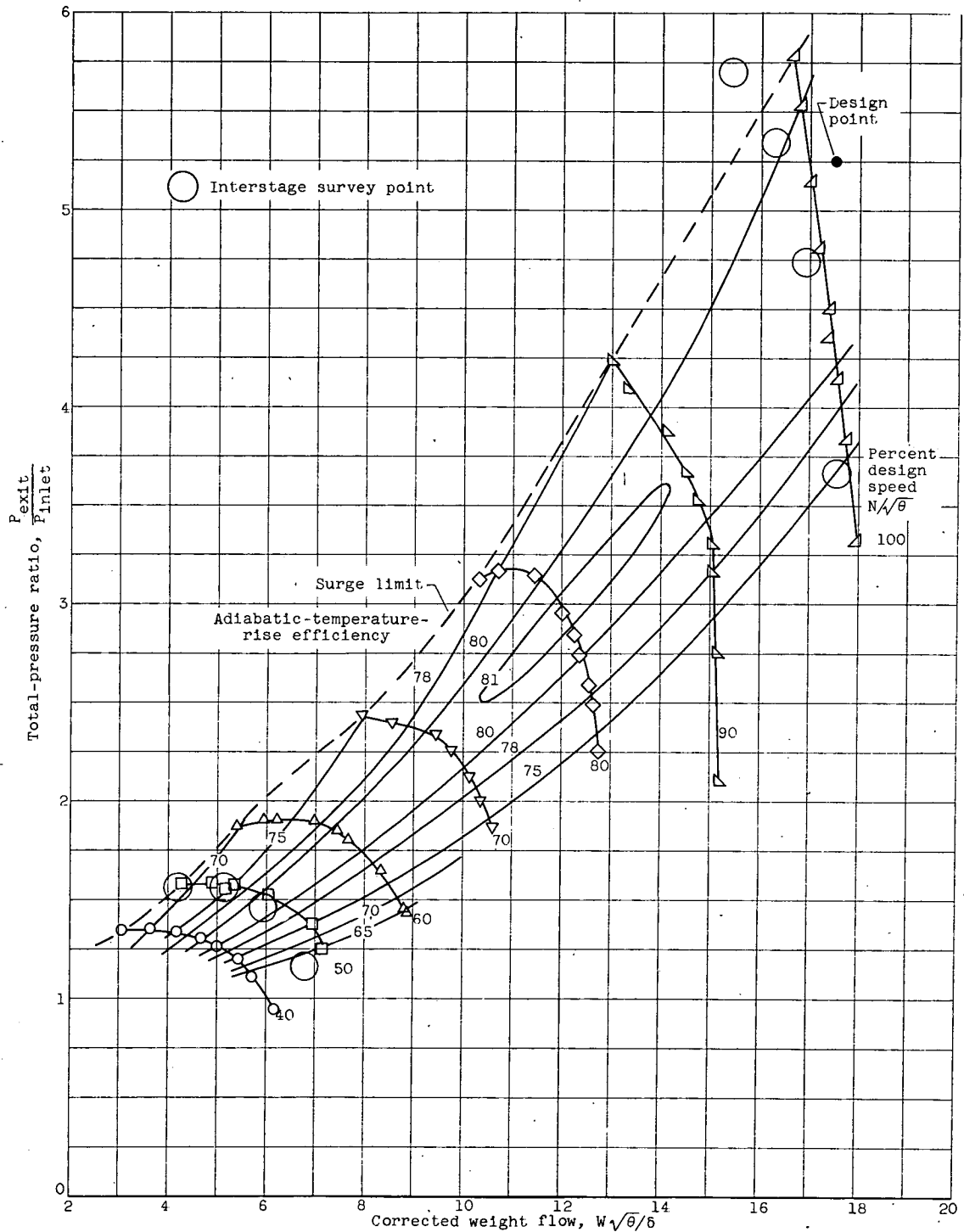
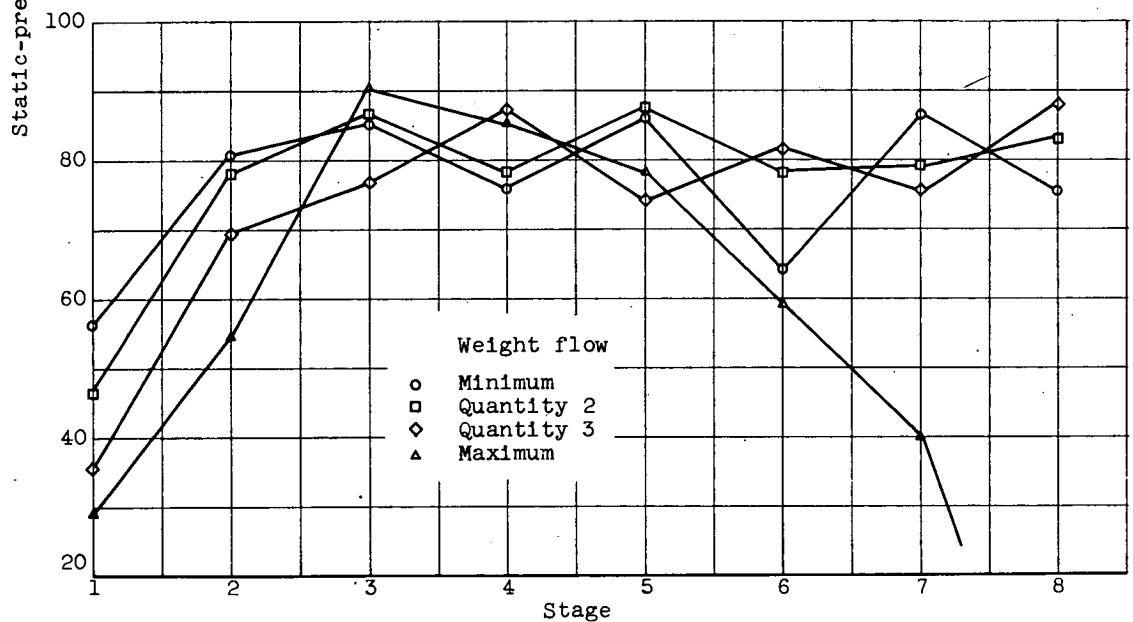


Figure 4. - Over-all performance map.



(a) 50 percent design speed.



(b) 100 percent design speed.

Figure 5. - Variation of static-pressure-rise efficiency through compressor.

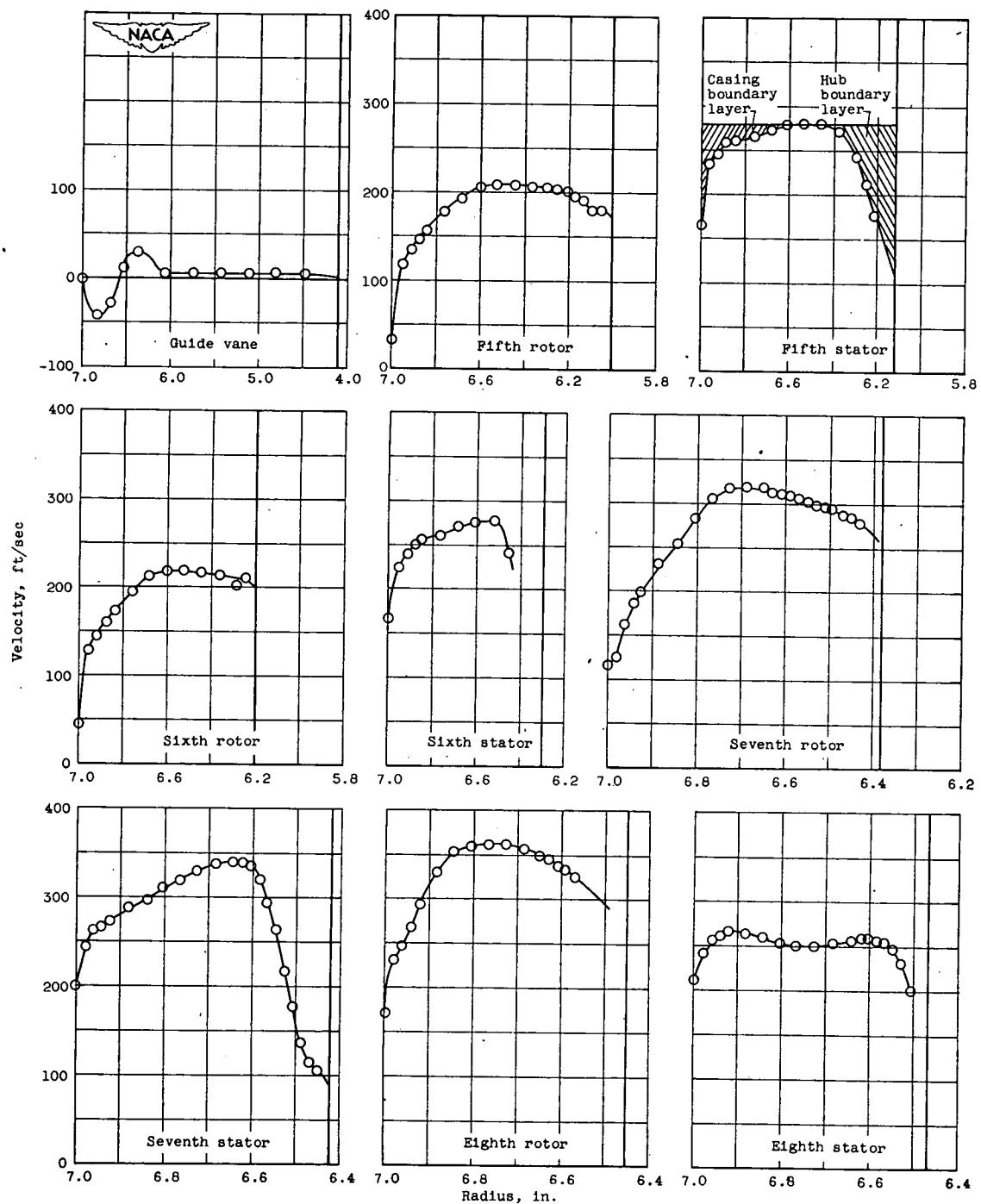
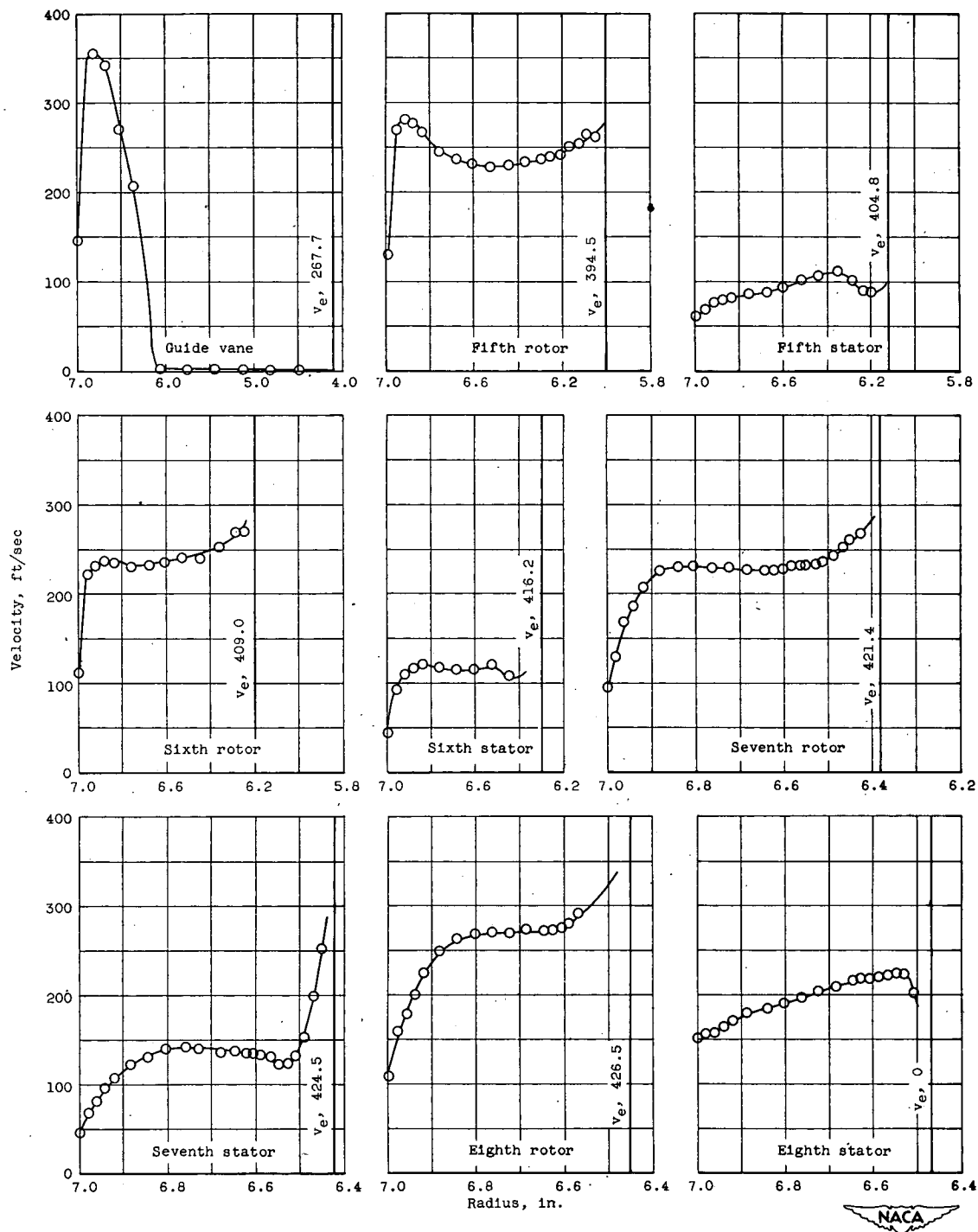
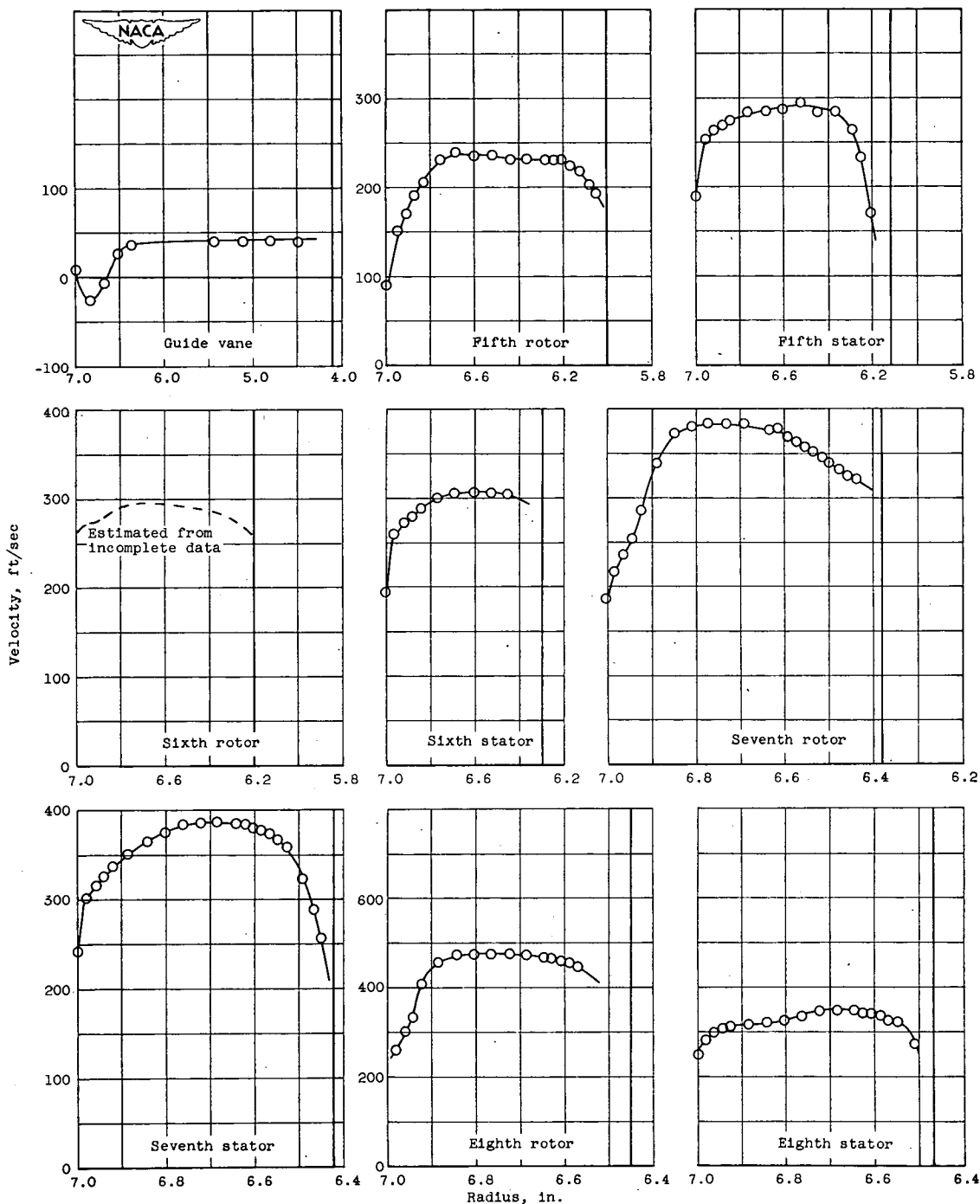


Figure 6. - Velocity profiles after indicated blade rows. Speed, 50 percent design.



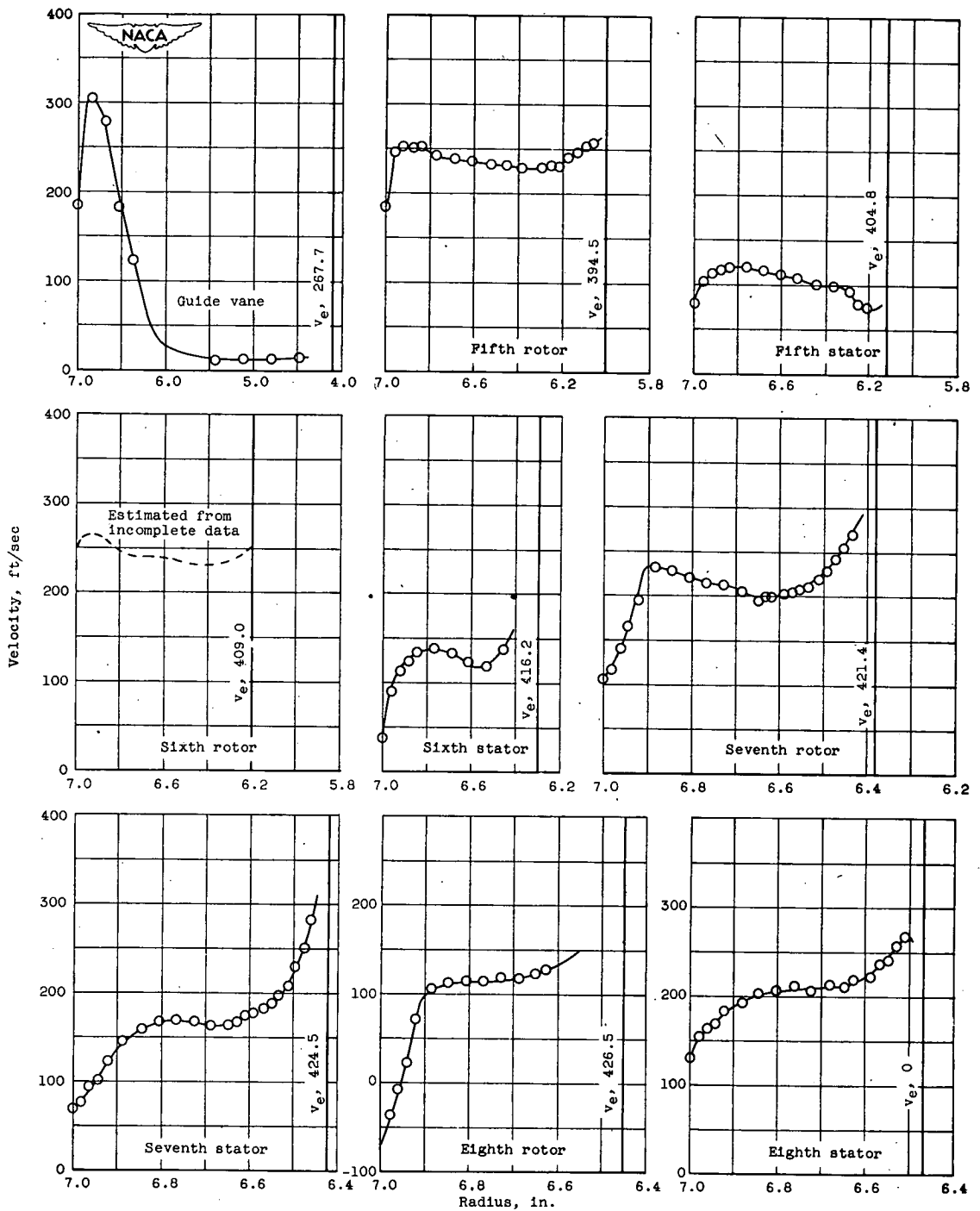
(b) Tangential velocity; minimum weight flow;  $v_e$ , equivalent tangential velocity of hub.

Figure 6. - Continued. Velocity profiles after indicated blade rows. Speed, 50 percent design.

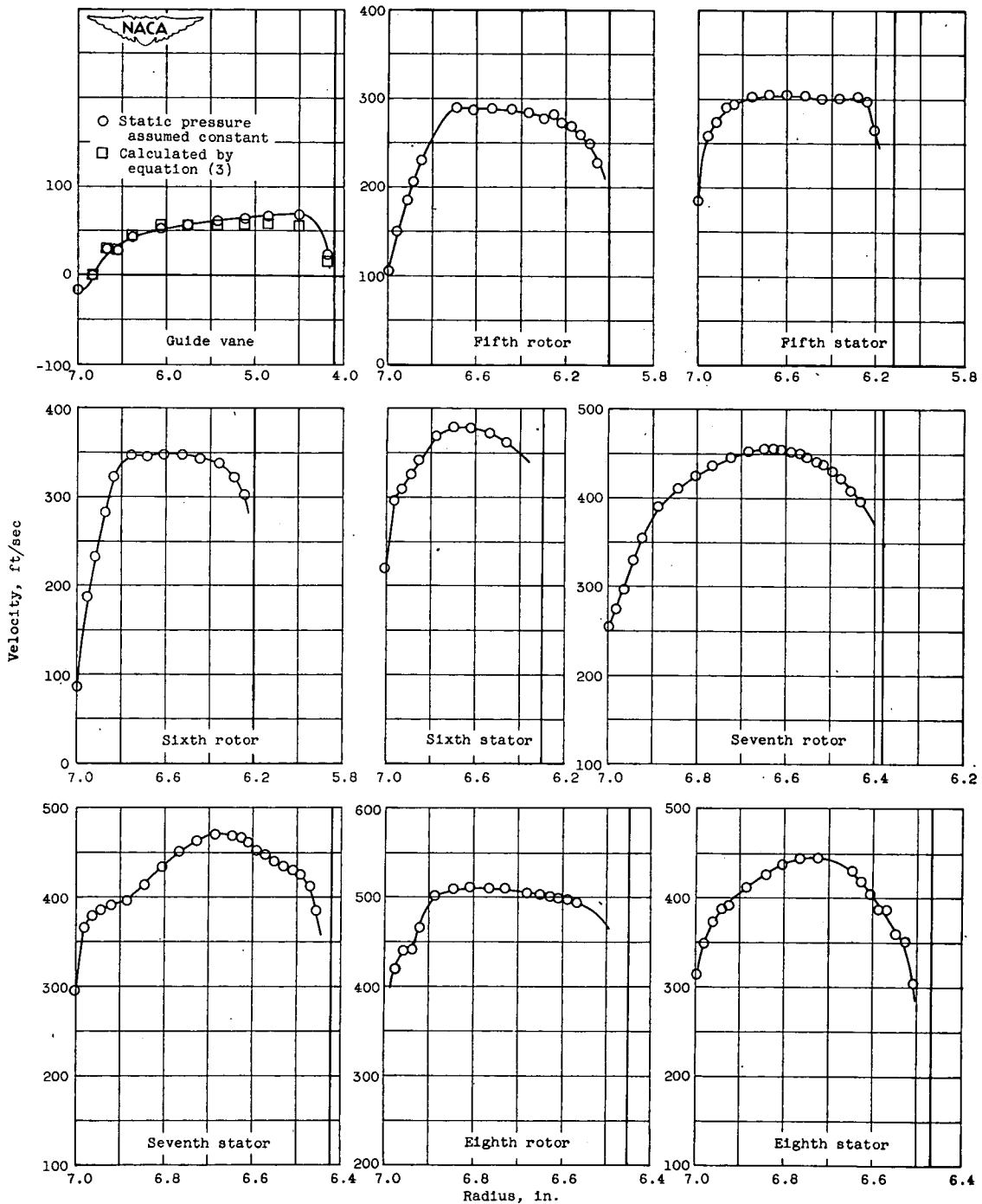


(c) Axial velocity; quantity 2 weight flow.

Figure 6. - Continued. Velocity profiles after indicated blade rows. Speed, 50 percent design.

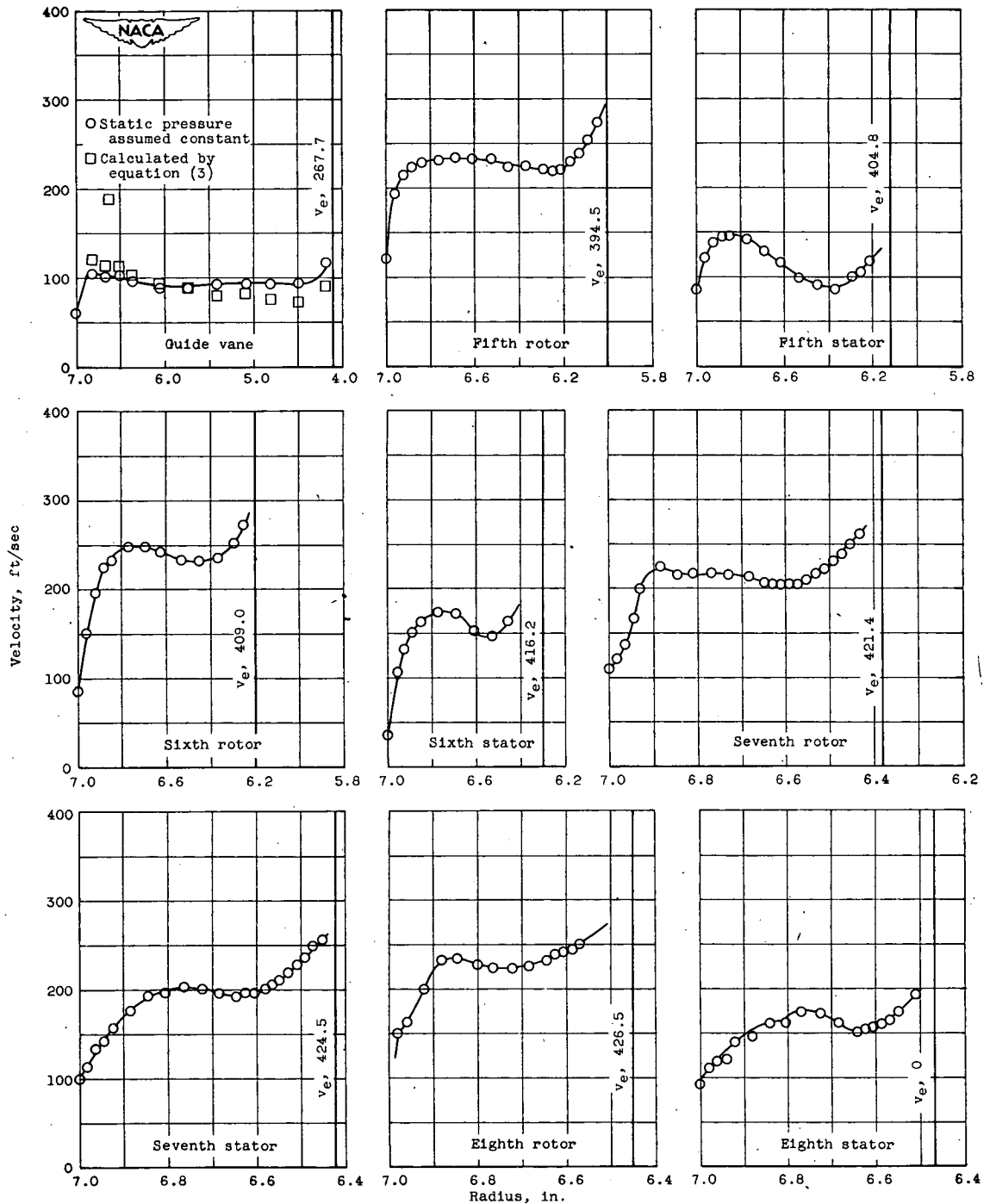


(d) Tangential velocity; quantity 2 weight flow;  $v_e$ , equivalent tangential velocity of hub.  
 Figure 6. - Continued. Velocity profiles after indicated blade rows. Speed, 50 percent design.

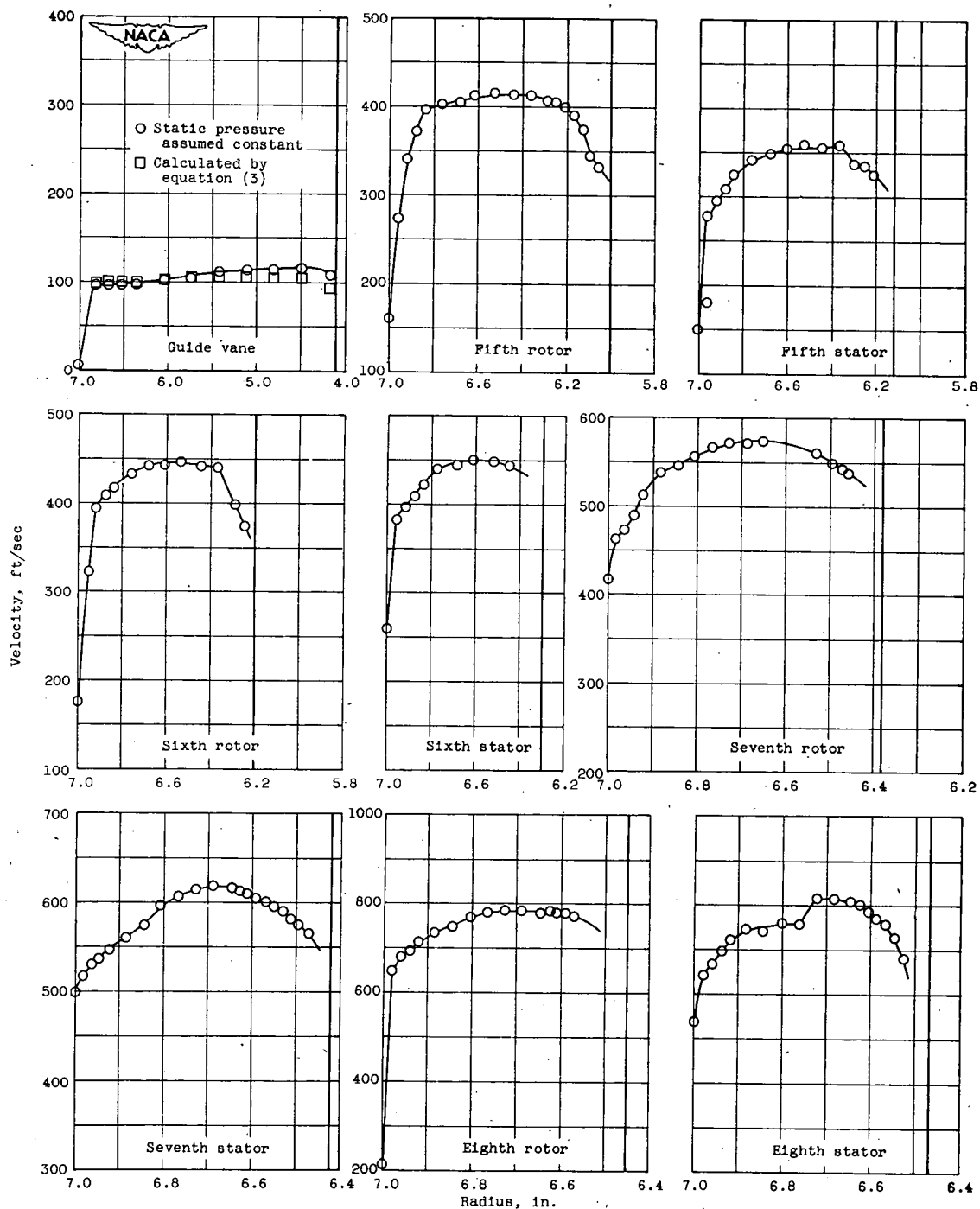


(e) Axial velocity; quantity 3 weight flow.

Figure 6. - Continued. Velocity profiles after indicated blade rows. Speed, 50 percent design.

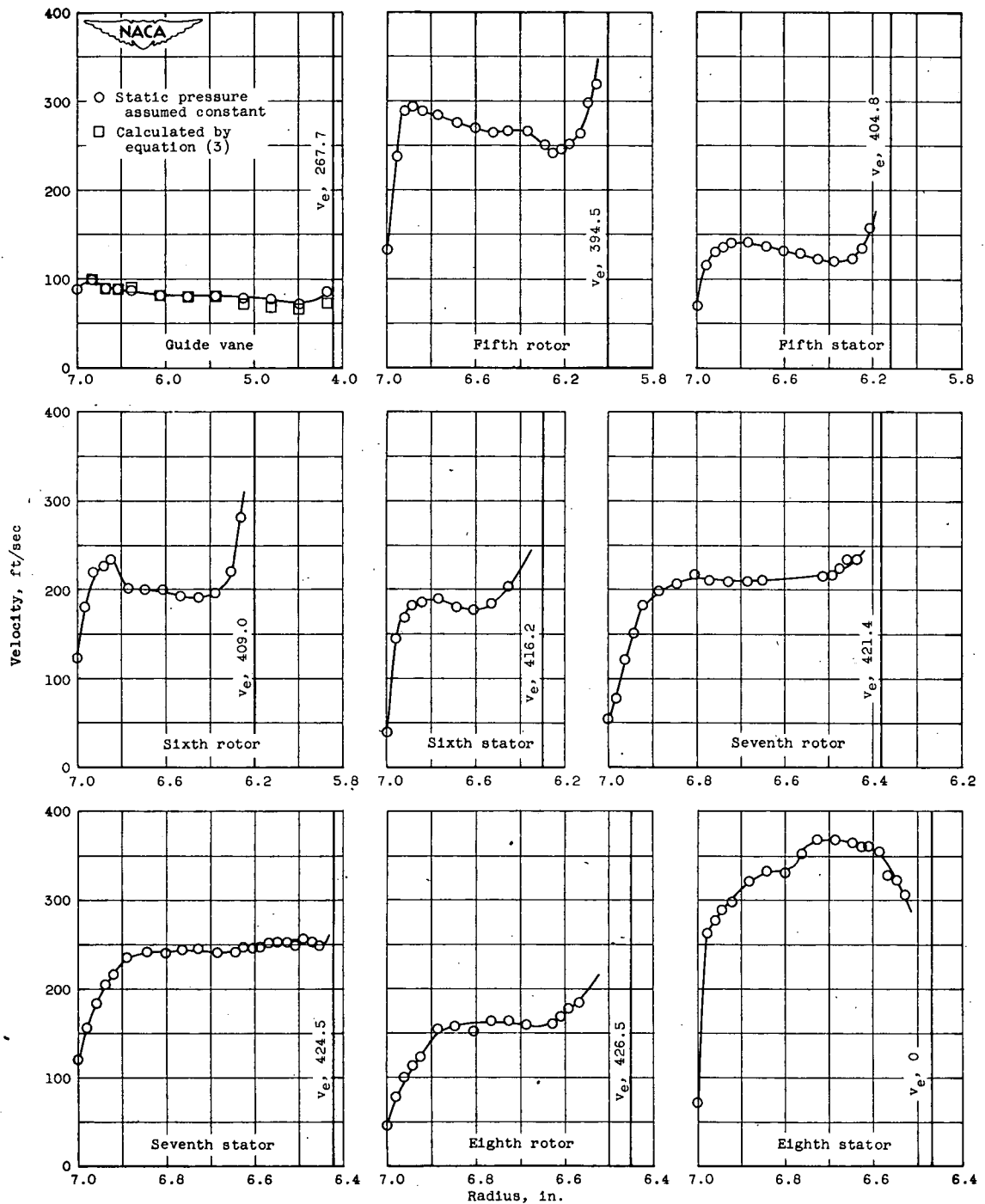


(f) Tangential velocity; quantity 3 weight flow;  $v_e$ , equivalent tangential velocity of hub.  
 Figure 6. - Continued. Velocity profiles after indicated blade rows. Speed, 50 percent design.



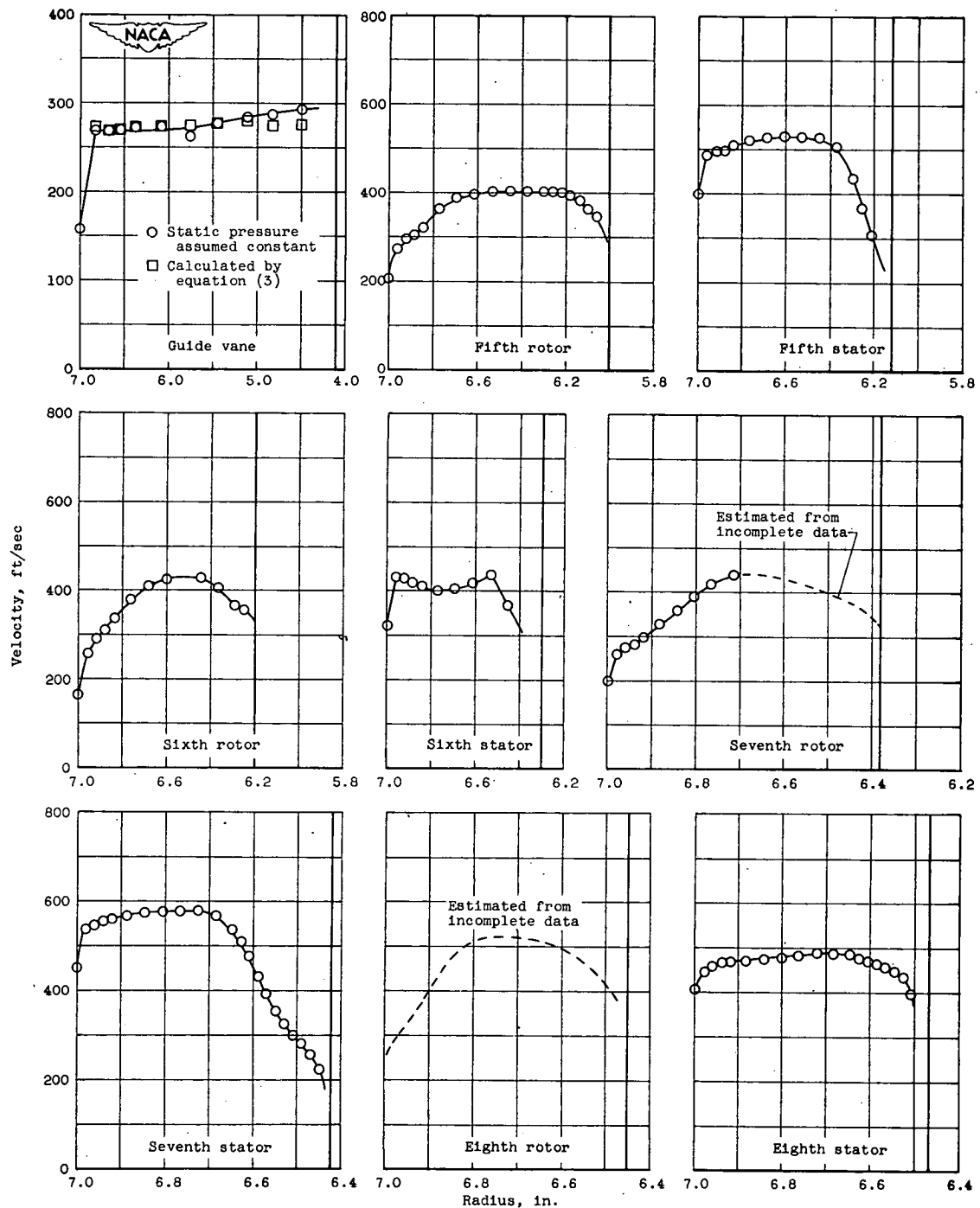
(g) Axial velocity; maximum weight flow.

Figure 6. - Continued. Velocity profiles after indicated blade rows. Speed, 50 percent design.



(h) Tangential velocity; maximum weight flow;  $v_e$ , equivalent tangential velocity of hub.

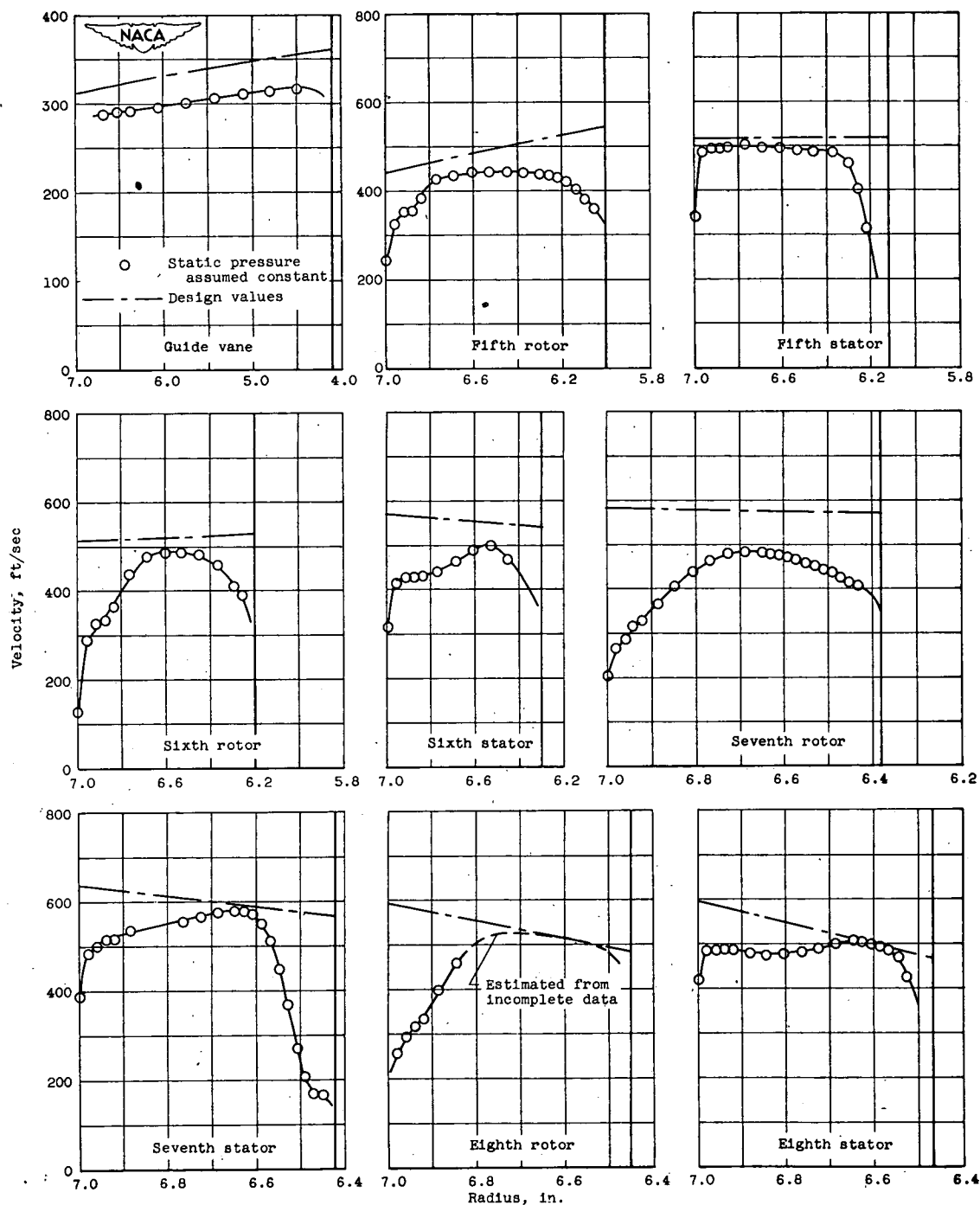
Figure 6. - Concluded. Velocity profiles after indicated blade rows. Speed, 50 percent design.



(a) Axial velocity; minimum weight flow.

Figure 7. - Velocity profiles after indicated blade rows. Speed, 100 percent design.





(c) Axial velocity; quantity 2 weight flow.

Figure 7. - Continued. Velocity profiles after indicated blade rows. Speed, 100 percent design.

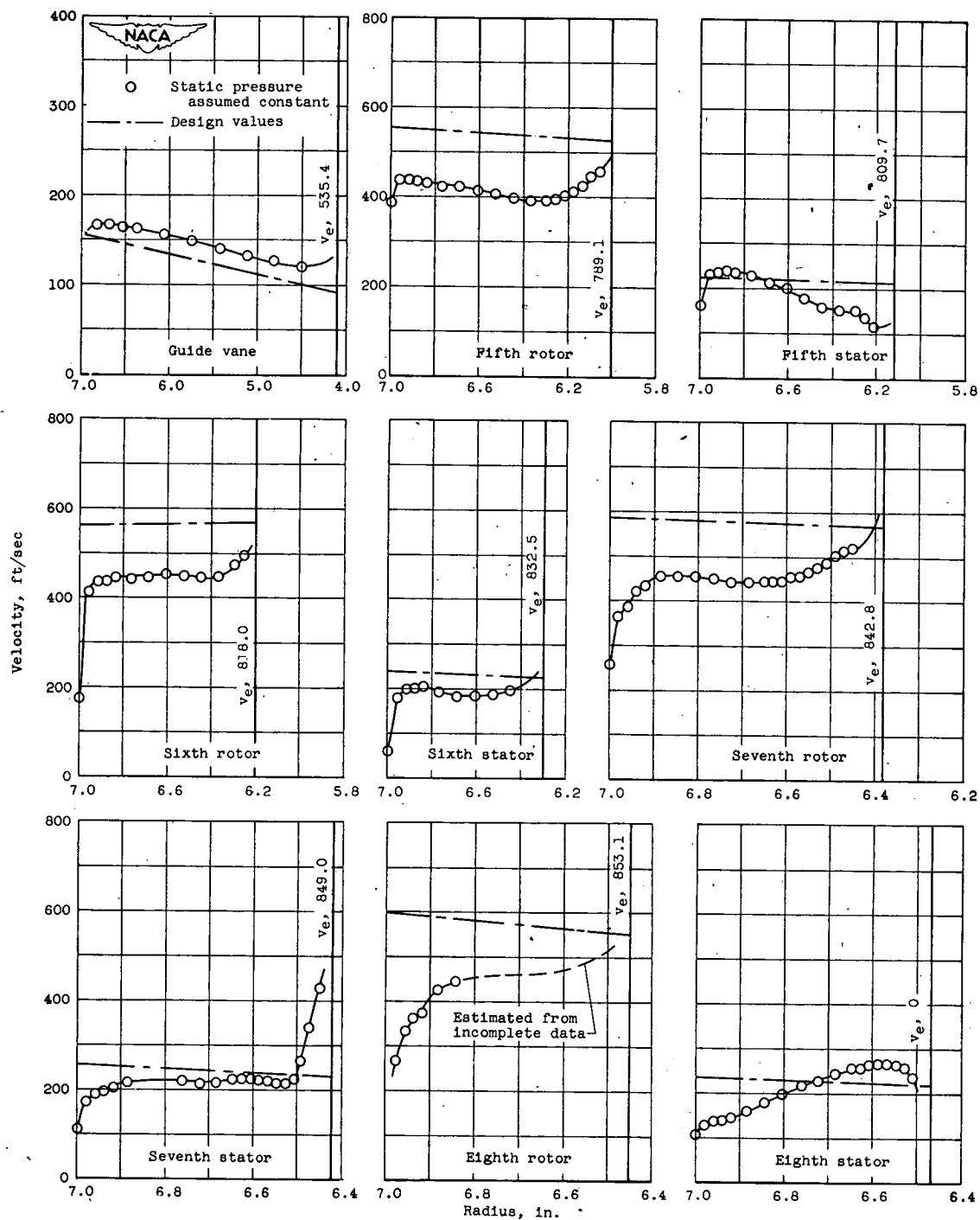
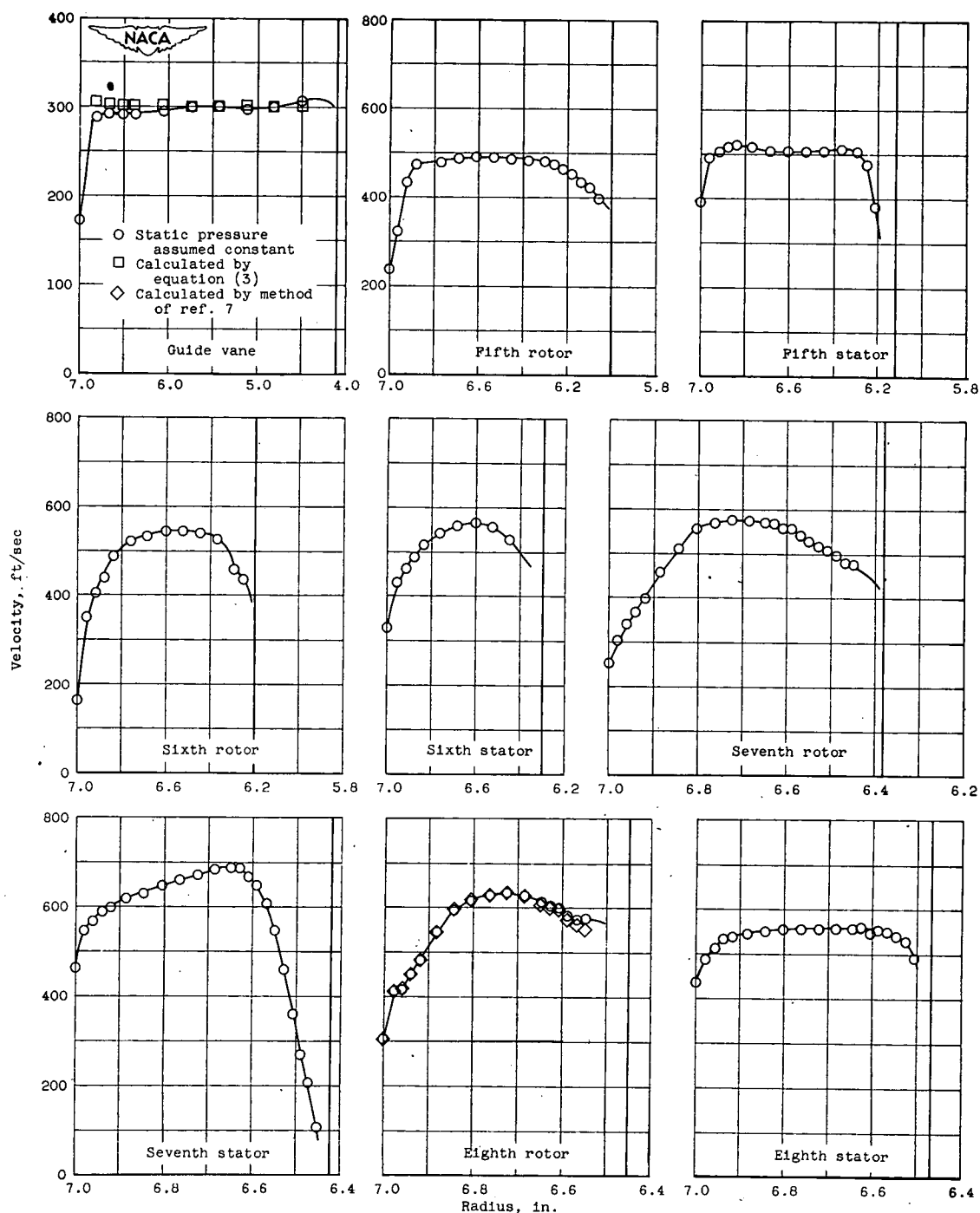
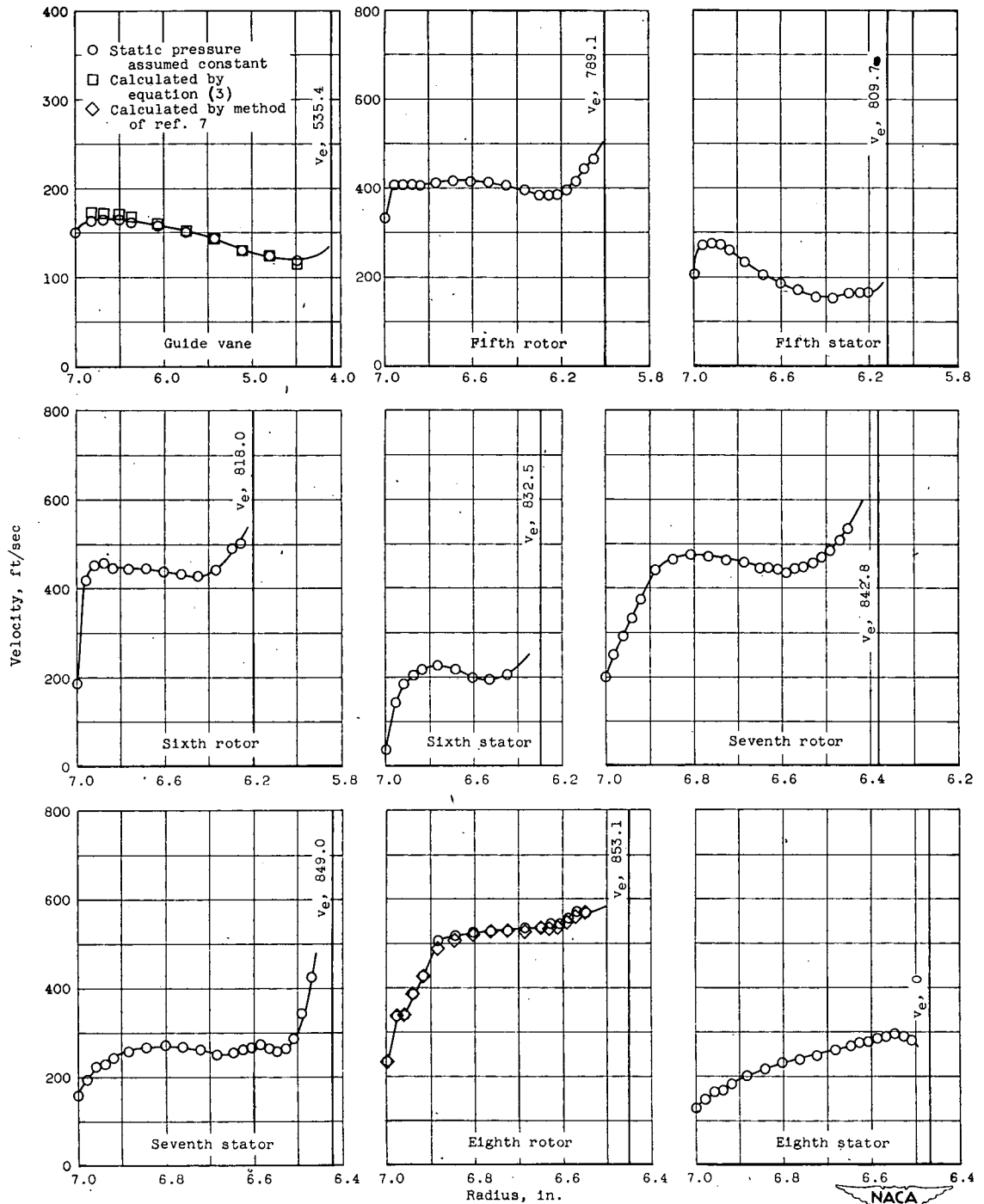


Figure 7. - Continued. Velocity profiles after indicated blade rows. Speed, 100 percent design.



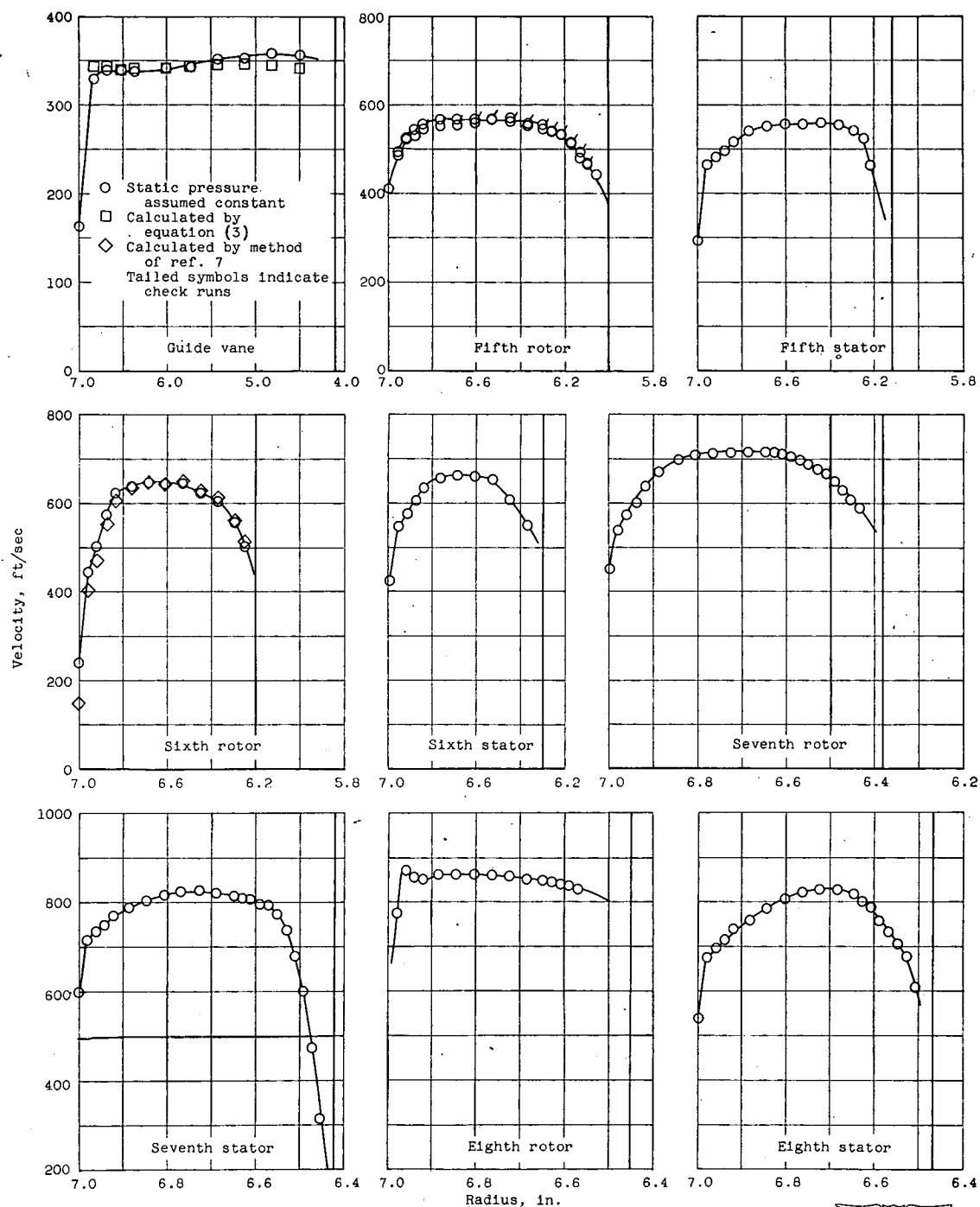
(e) Axial velocity; quantity 3 weight flow.

Figure 7. - Continued. Velocity profiles after indicated blade rows. Speed, 100 percent design.



(f) Tangential velocity; quantity 3 weight flow;  $v_e$ , equivalent tangential velocity of hub.

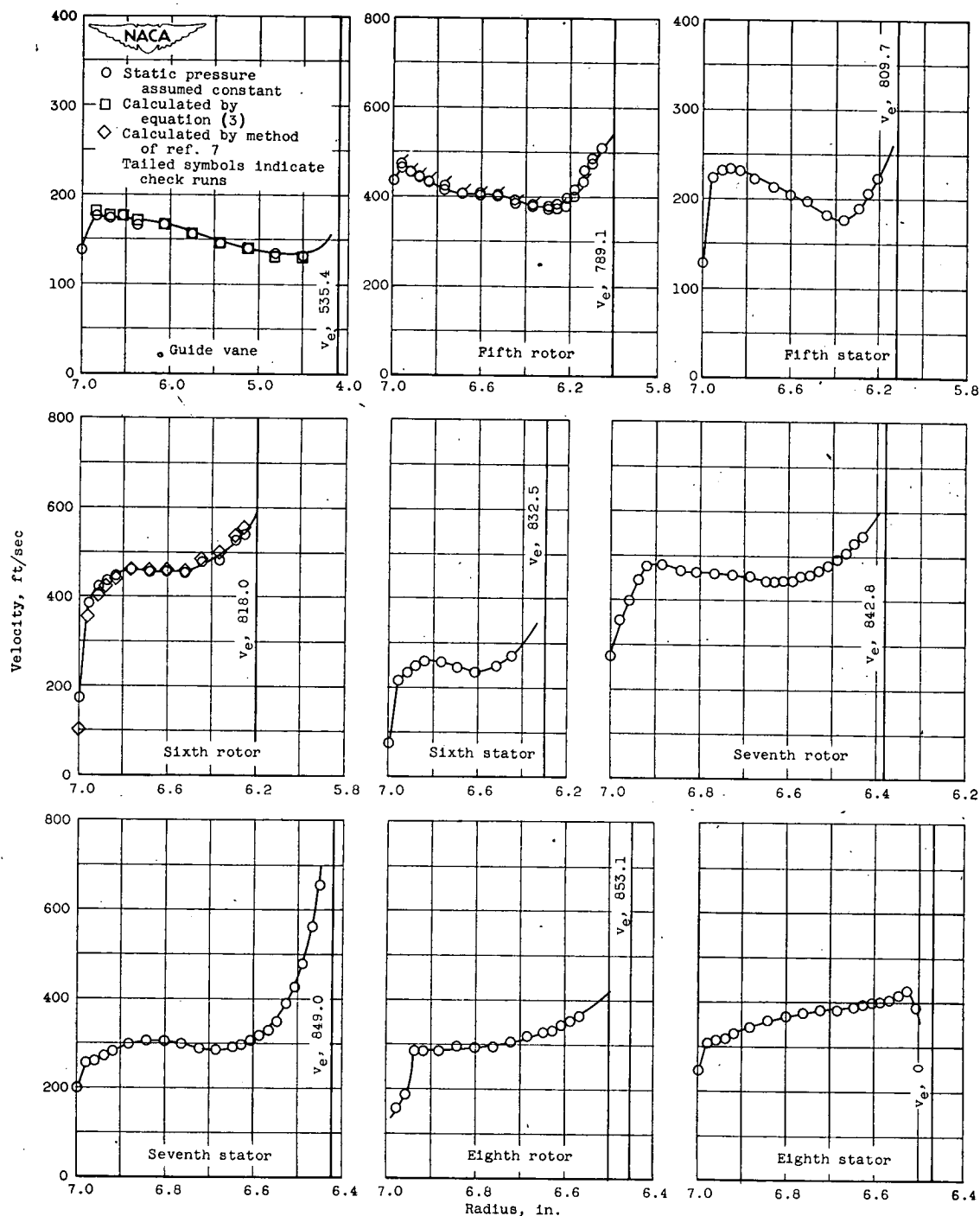
Figure 7. - Continued. Velocity profiles after indicated blade rows. Speed, 100 percent design.



(g) Axial velocity; maximum weight flow.

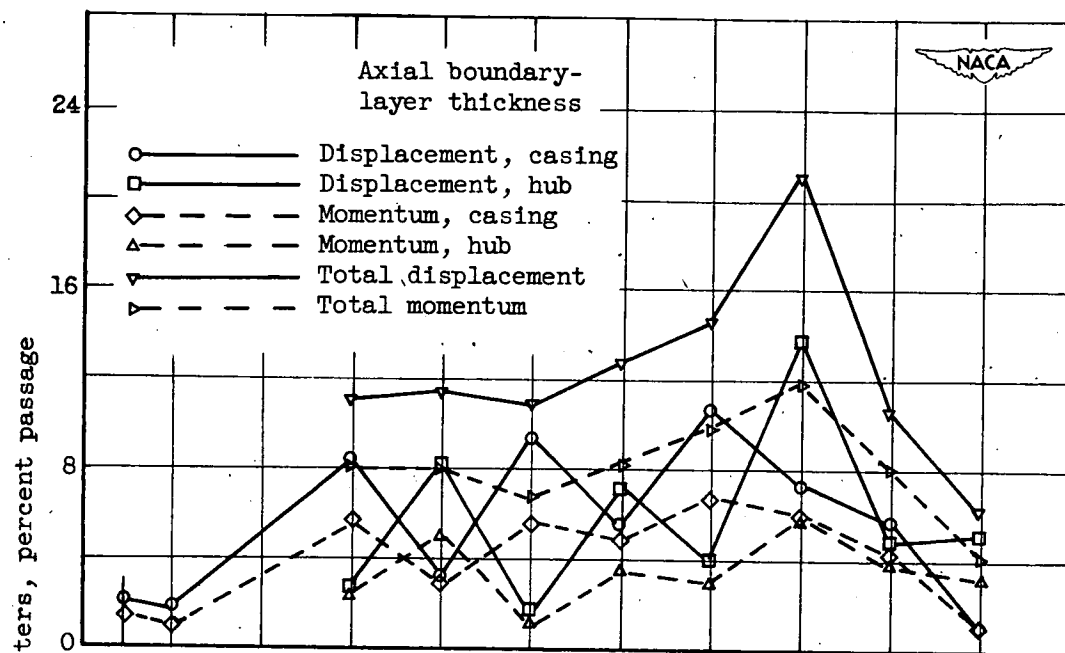


Figure 7. - Continued. Velocity profiles after indicated blade rows. Speed, 100 percent design.

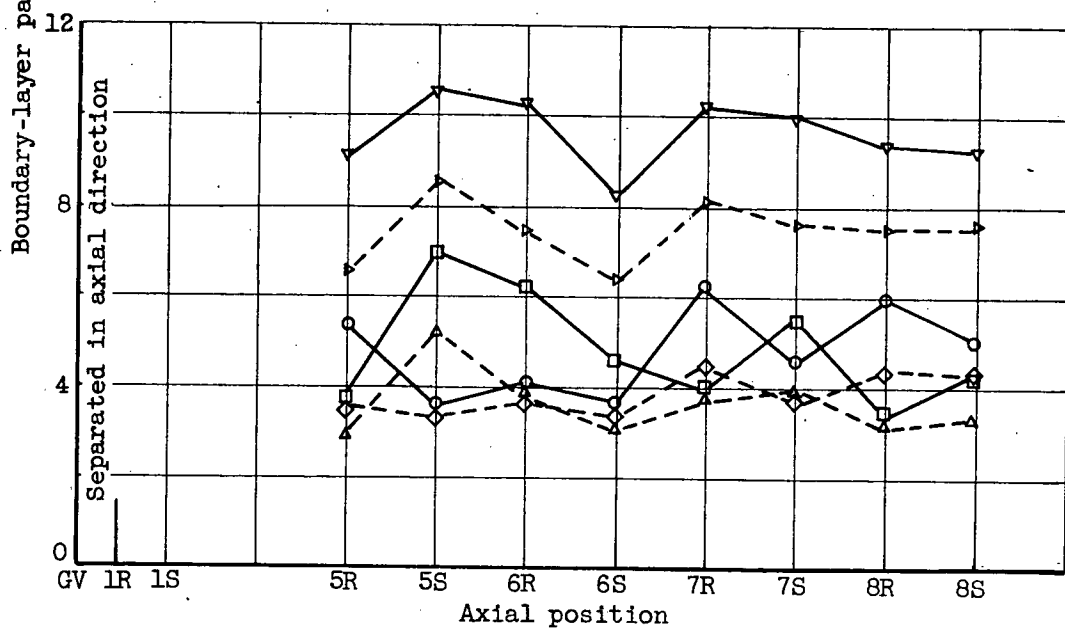


(h) Tangential velocity; maximum weight flow;  $v_e$ , equivalent tangential velocity of hub.

Figure 7. - Concluded. Velocity profiles after indicated blade rows. Speed, 100 percent design.



(a) Minimum weight flow.



(b) Quantity 2 weight flow.

Figure 8. - Values of boundary-layer thickness through compressor at 50 percent design speed. GV, guide vane; R, rotor; S, stator.



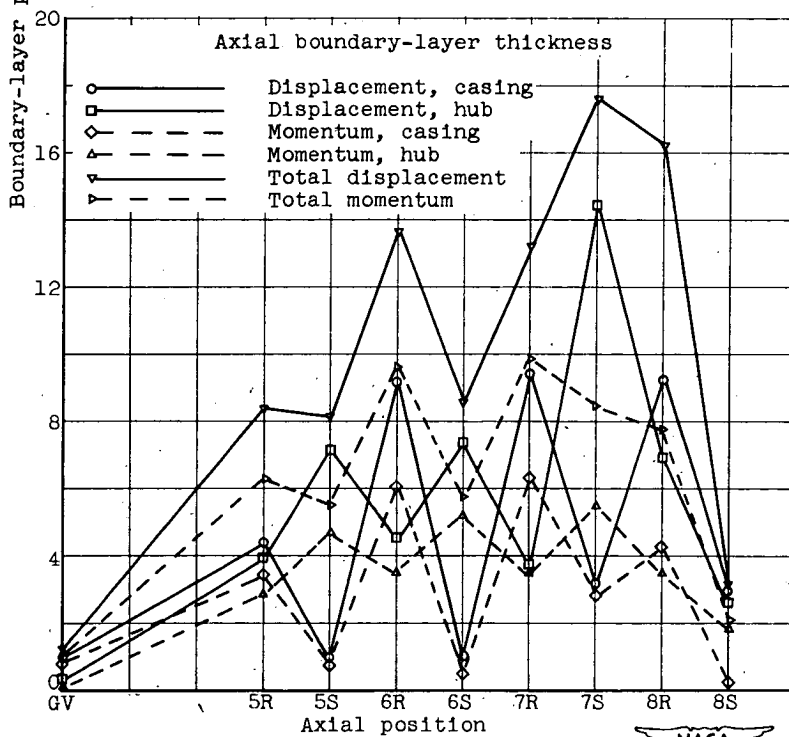
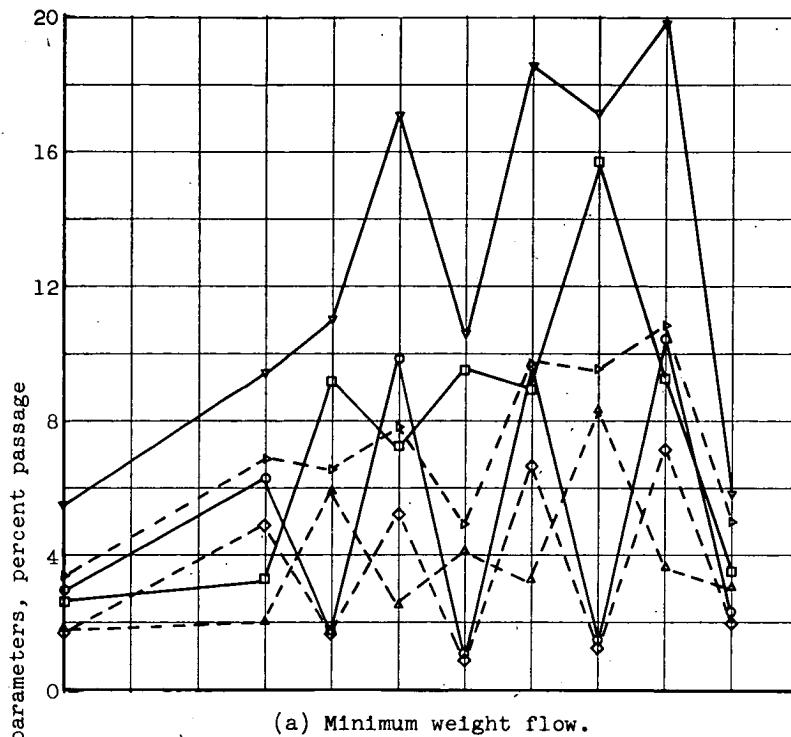


Figure 9. - Values of boundary-layer thickness through compressor at 100 percent design speed. GV, guide vane; R, rotor; S, stator.

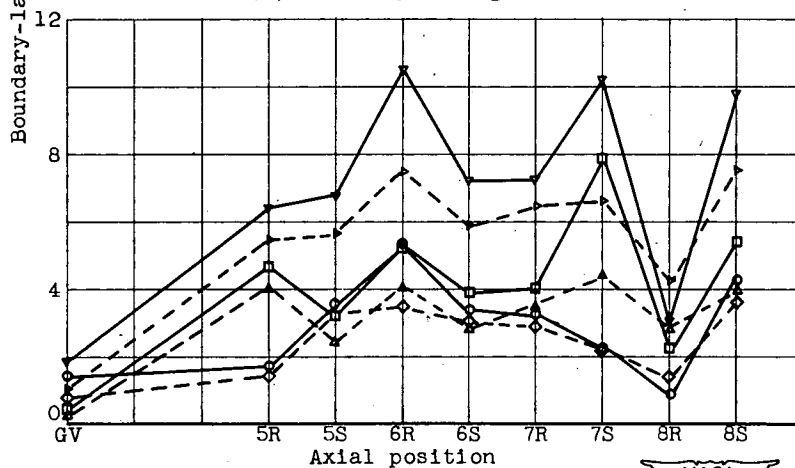
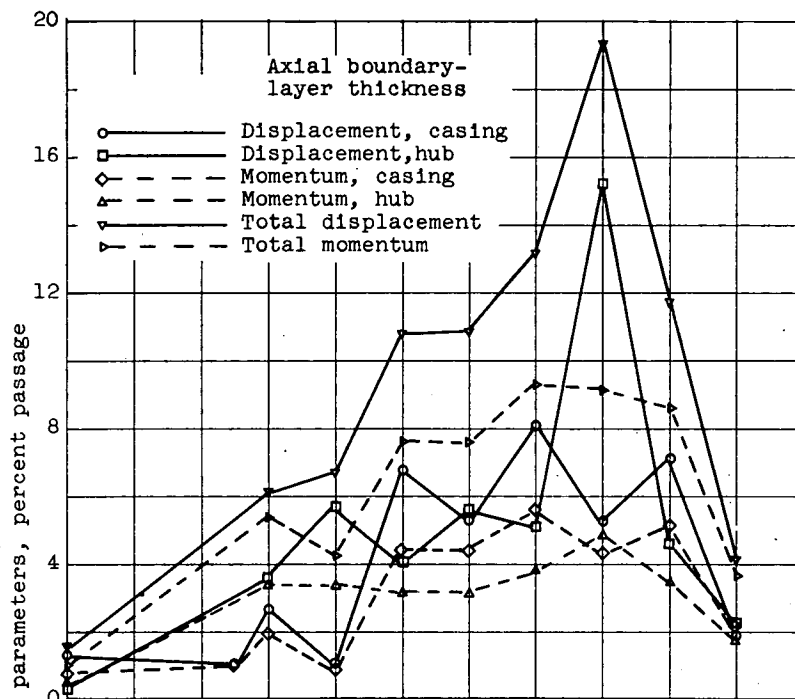
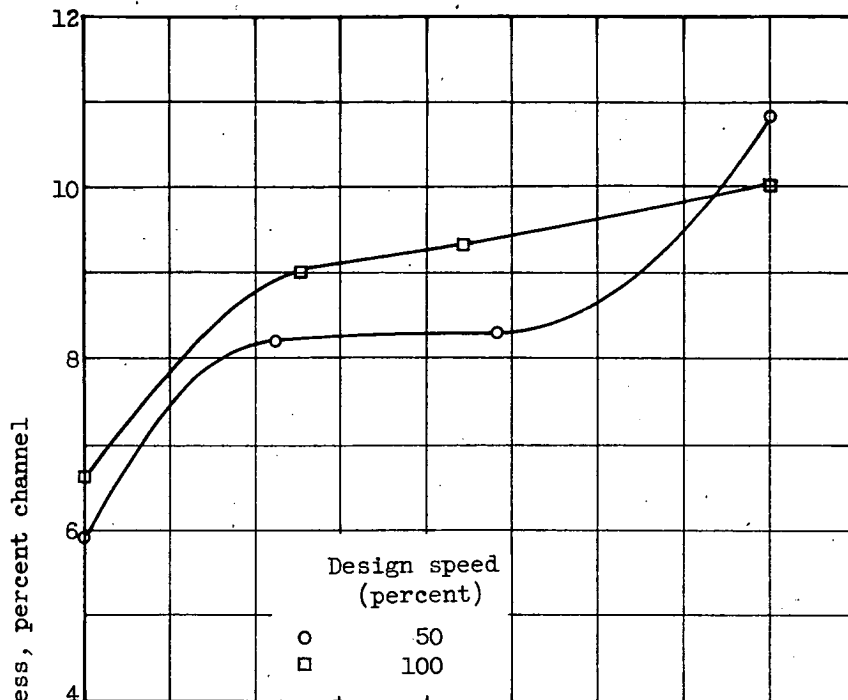
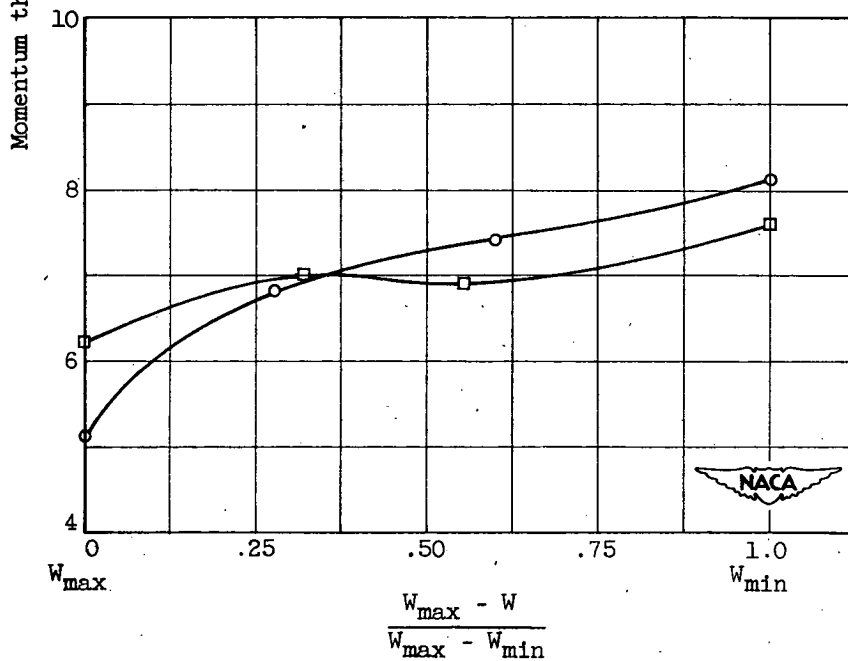


Figure 9. - Concluded. Values of boundary-layer thickness through compressor at 100 percent design speed. GV, guide vane; R, rotor; S, stator.



(a) Reasonable maximum momentum thickness.



(b) Average momentum thickness.

Figure 10. - Variation of maximum-momentum-thickness values in last four stages with mass flow and speed.

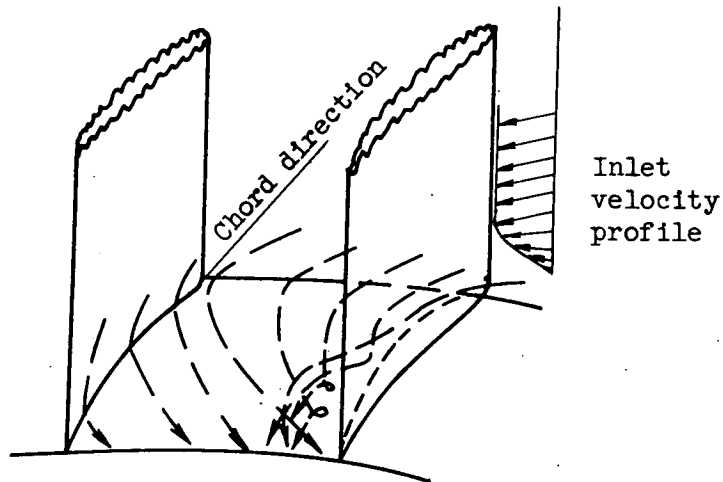


Figure 11. - Secondary flow deflections in curving channel.

Stationary casing and stator blades

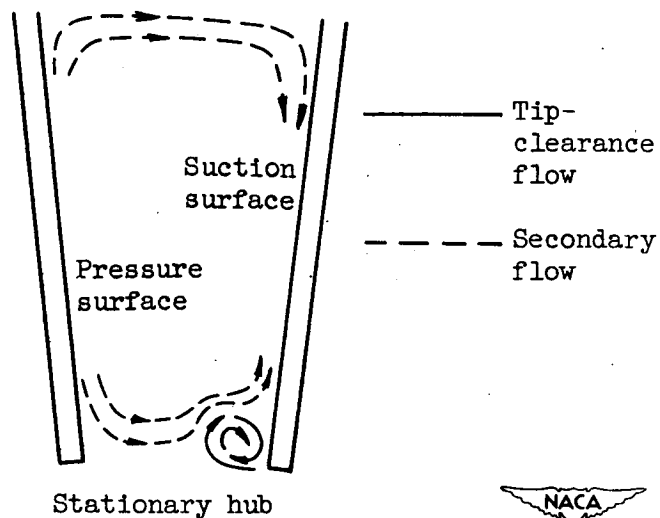


Figure 12. - Looking upstream at flow motions in blade passages produced by tip-clearance flow and its interaction with secondary flow with no relative motion between blades and walls.

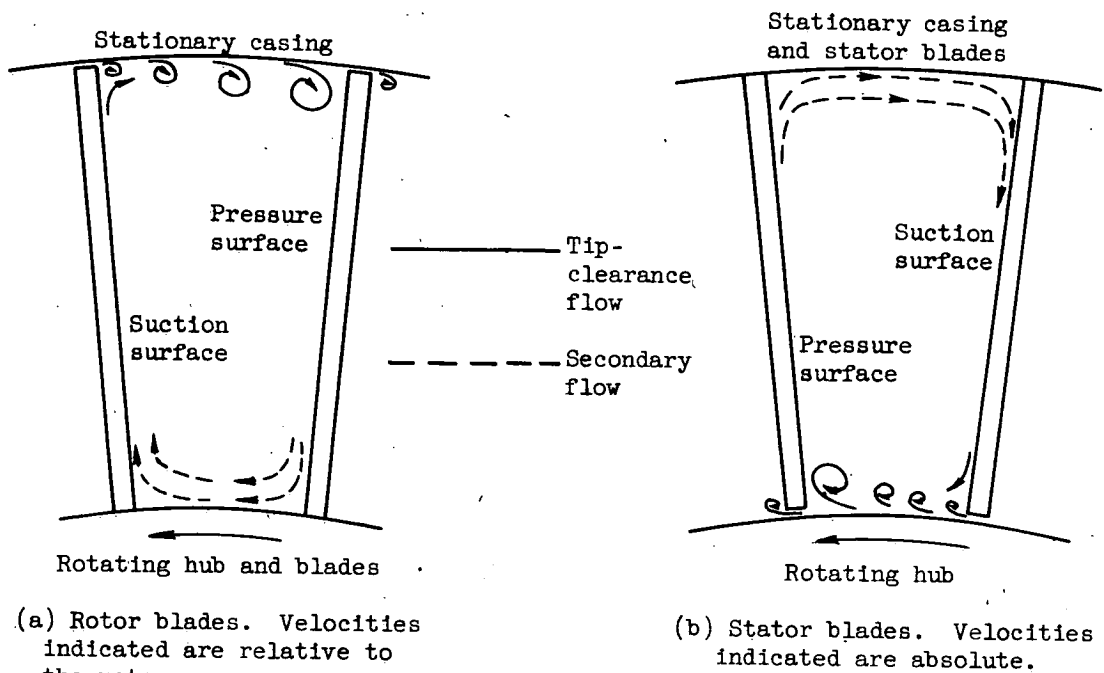


Figure 13. - Looking upstream at flow motions in blade passages produced by tip-clearance flow and its interaction with secondary flow.

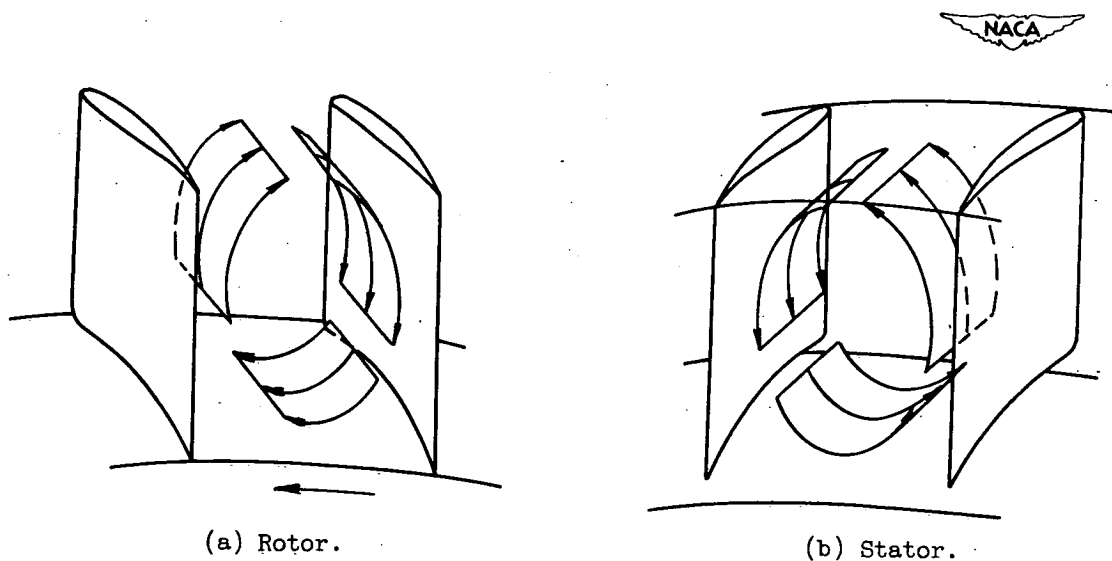


Figure 14. - Flow motion induced by rotating coordinate frame (with no through flow).

# SECURITY INFORMATION

~~CONFIDENTIAL~~

1  
1  
2  
1

ALL INFORMATION CONTAINED  
HEREIN IS UNCLASSIFIED  
DATE 10/1/00 BY 1043  
1043

~~CONFIDENTIAL~~